Diagenesis and its impact on the reservoir quality of Miocene sandstones (Surma Group) from the Bengal Basin, Bangladesh

M. Julleh J. Rahman[1] and Richard H. Worden[2*]

[1]Dept. of Geological Sciences, Jahangirnagar University, Dhaka, Bangladesh

[2] Dept. of Earth, Ocean and Ecological Sciences, University of Liverpool, L69 3GP, United Kingdom

Abstract

Rapid supply and deposition of 1000's of meters of Miocene and Pliocene sediment tend to lead to a different set of controls on reservoir quality than older, more slowly buried sandstones. Here we have studied Miocene fluvial-deltaic Bhuban Formation sandstones, from the Surma Group, Bengal Basin, buried to >3,000m and >110ºC, using a combination of petrographic, geochemical and petrophysical methods in order to understand the controls on Miocene sandstone reservoir quality to facilitate improved prediction of porosity and permeability. The main conclusions of the study are that mechanical compaction processes are the dominant control on porosity-loss although early calcite growth has led to locally-negligible porosity in some sandstones. Mechanical compaction occurred by grain rearrangement, ductile grain compaction and brittle grain fracturing. Calcite cement, occupying up to 41% intergranular volume, was derived from a combination of dissolved and recrystallized bioclasts, an influx of organic-derived carbon dioxide and plagioclase alteration. Clay minerals present include smectite-illite, kaolinite and chlorite. The smectitic clay was probably restricted to low energy depositional environments and it locally diminishes permeability disproportionate to the degree of porosity-loss. Kaolinite is probably the result of feldspar alteration resulting from the influx of organic-derived carbon dioxide. Quartz cement is present in small amounts, despite the relatively high temperature, due to a combination of limited time available in these young sandstones, grain-coating chlorite and low water saturations in these gas-bearing reservoir sandstones. Reservoir quality can now be predicted by considering primary sediment supply and primary depositional environment, the magnitude of the detrital bioclast fraction and the influx of organic-derived carbon dioxide.

Key words: Diagenesis; sandstone; reservoir quality; Miocene; Surma Group; Bengal Basin; mechanical compaction, calcite cement

*Corresponding author. E-Mail. r.worden@liverpool.ac.uk, UK-44 1517945184

1. Introduction

The Bengal Basin in Southeast Asia covers most of Bangladesh and is known as a prolific petroleum-bearing basin. It contains up to 22,000 m of Cretaceous to Holocene sedimentary fill (Alam et al., 2003). This huge succession includes about ~4,000 to 5,000 m of Neogene sediment of the petroliferous Surma Group (Table 1) buried to 2,300 to 3,100 m. So far, twenty-five economically-viable fields have been discovered in Bangladesh. Predominantly, these are gas fields in the Miocene Surma Group sandstones. These recently-discovered gas fields have become a significant source of hydrocarbon in the Bengal Basin and promise to serve as an engine of economic growth for Bangladesh. There are several publications that have dealt with the regional geology, sedimentology, tectonic evolution and petroleum prospectivity of the Surma Basin, especially for the north-eastern petroleum province (Hiller and Elahi, 1984; Johnson and Alam, 1991; Khan et al., 1988; Lietz and Kabir, 1982; Rahman et al., 2009; Shamsuddin et al., 2001). However, relatively few publications focus on the reservoir quality and diagenesis of the sandstone units (Imam and Shaw, 1987; Islam, 2009; Rahman and McCann, 2012; Rahman et al., 2011).

Reservoir quality (porosity and permeability) is a key control on success during petroleum exploration, along with source presence, maturation, migration, trap and seal. Reservoir quality is a function of primary sand texture and composition and the secondary diagenetic processes of compaction, mineral cementation, mineral replacement and mineral dissolution (Worden and Burley, 2003). The necessarily limited time available to bury Miocene sediment to >2,000 m requires either a very large river system spewing sediment into a basin with a restricted dimensions, or a major tectonic event (e.g. the Himalayan orogeny) in the sediment's hinterland (or a combination of both reasons). The Bengal Basin has accumulated sediment at about 150 m/myr, a value that is approximately ten times greater than, for example, the rate of sediment accumulation for the Brent Group reservoirs in the North Sea. There are some notable differences in the controls on reservoir quality in Neogene sandstones at ~2,000 to 3,500 m compared to Palaeogene or older sandstones, at equivalent depths, due to the accelerated rate of sediment supply and burial. The rapid burial and consequent heating of Miocene sediments to > 2,300 m suggests that kinetically-controlled diagenetic processes, for example carbonate neoformation, clay mineral transformations or the growth of quartz cement, will be less advanced than in older basins at the same depth and temperature (Dutton et al., 2012; Gier et al., 2008). Furthermore if a major Miocene tectonic event led to the supply of a vast amount of sediment from the surrounding mountain belts, it is likely that the supplied sediment will be mineralogically immature compared to sediment supplied and accumulated more slowly (Worden et al., 2000; Worden et al., 1997). Therefore, it is important to have a detailed understanding of sandstone diagenesis during petroleum exploration in young, e.g. Miocene, basins. Previous studies on diagenetic cements in the Bengal Basin revealed a dominant presence of calcite cement in the Surma Group (Rahman and McCann, 2012). The present investigation is a petrographic and geochemical study of Surma Group sandstones dominantly from the central Bengal Basin. It builds on earlier work (Imam and Shaw, 1987; Islam, 2009; Rahman and McCann, 2012; Rahman et al., 2011) by undertaking a full assessment of all the possible controls on reservoir quality, extending the study to a great range of depths (2303 m to 3178 m; Fig. 2), using stable isotope data from calcite cement from the central Bengal Basin and, for the first time, incorporating core analysis data. Samples have been collected from six exploration wells from four gas fields (Jalalabad, Meghna, Narsingdi, SaldaNadi and Titas; Fig. 1).

This paper specifically seeks to address the following research questions:

1) Is compaction or cementation the dominant control on reservoir quality in young (Miocene) sandstones buried to more than 3,000 m?

2) What are the main sources of carbonate cement in these young and deeply buried sandstones and can we predict this control on reservoir quality?
3) Is quartz cement common in these young sandstones heated to more than 100C°?
4) What are the key aspects of diagenesis to consider in an assessment and prediction of reservoir quality of young sandstones buried to more than 3,000 m and heated to more than 100C°?

2. Geological setting

The Cretaceous to Holocene Bengal Basin lies on the eastern side of the Indian subcontinent between the Shillong Plateau to the north, and the Indo-Burman Ranges to the east. The Bengal Basin occupies most of Bangladesh and West Bengal (India) as well as part of the Bay of Bengal (Fig. 1). Basin development is concluded to have started in the Early Cretaceous epoch (ca. 127 Ma) when the Indian plate rifted away from Antarctica, although there is ongoing debate about the precise timing of rifting (Gibbons et al., 2013; Jokat et al., 2010). After plate reorganization at about 90 Ma, the Indian plate migrated rapidly northward and collided with Asia between approximately 55 and 40 Ma (Johnson and Alam, 1991). This basin originated during the collision of India with Eurasia and Burma, building the extensive Himalayan and Indo-Burman mountain ranges and, thereby, loading the lithosphere to form flanking sedimentary basins (Uddin and Lundberg, 1998).

Since the Cretaceous, sedimentation in the Bengal Basin has been controlled by the movement and collision pattern of the Indian plate with the Burmese and Tibetan plates and by the uplift and erosion of the Himalayas and Indo Burman Ranges (Alam, 1989). The basin-fill of the onshore part of the basin has previously been divided into platform (shelf), slope (hinge) and basinal facies (Alam et al., 2003) (Fig. 1). Crystalline basement of the Indian plate underlies the shelf and bounds the Bengal Basin to the west and north; the deeper basin to the east and southeast may be floored by oceanic or transitional crust (Johnson and Alam, 1991).

Upper Cretaceous to Middle Eocene stratigraphic units comprise non marine to shallow-marine deposits (Uddin and Lundberg, 1998). Basin-wide subsidence took place in the middle Eocene resulting an extensive marine transgression with the deposition of the nummulitic Sylhet Limestone Formation (Table 1). This event was followed by the brackish to marine shales of Kopili Formation. In the Oligocene, basin-wide emergence and marine regression occurred, followed by deposition of the Barail Group.

During the Miocene, major uplift began in Himalayas, and large volumes of orogenic sediments were funneled into the basin from the north east, building a major Mio-Pliocene delta complex (Uddin and Lundberg, 1998). The Miocene Surma Group was then deposited in deltaic to shallow marine environments followed by predominantly fluvial deposition of the Mio-Pliocene Tipam Formation and then finally fluviatile Plio-Pleistocene Dupi Tila Formation sandstones (Alam, 1989).

The sediments of the Miocene Surma Group have been sub-divided into, in age order, the Bhuban and Boka Bil Formations. The wells utilized in this study had reservoirs in the Bhuban Formation (Fig. 2). The Bhuban and Boka Bil Formations were principally deposited in a large, mud-dominated delta system that drained a significant portion of the eastern Himalaya (Johnson and Alam, 1991). The delta responsible for the Surma Group has been interpreted to be tide-dominated (Alam, 1995; Rahman et al., 2009). The marine-deltaic to fluvial-deltaic shale and sandstone rhythmites of the Surma Group sediments are reported to represent repetitive transgression and regression phases that resulted from subsidence as well as relative sea-level changes (Rahman et al., 2009) (Table 1). The older Bhuban Formation consists of fine grained, well-indurated, thickly bedded sandstones, siltstones, shales and claystones (Imam and Shaw, 1987). The reservoir sandstones of the Bhuban Formation of the Surma Group are characterized by a combination of massive units, parallel-lamination, cross-bedding, cross-bedded sandstones with lags of mud clasts, and ripple-lamination with flaser bedding (Rahman et al., 2009).

The borehole-temperature in the Bhuban Formation sandstones in this study range from 85°C at 2300 m to 115°C at 3200 m. Burial history and thermal modelling indicate that the main phase of oil and gas generation occurred around 12 million years ago (BAPEX, 1996) (Fig. 3). The sandstones have not been reported to be significantly overpressured.

3. Samples and methods

Thin section petrographic analysis was performed on 85 sandstone core samples collected at a range of depths between 2303 m and 3178m from six exploratory wells from four gas fields: Jalalabad (JL-2, JL-3, both drilled in 1989), Meghna (BK-9, 1990), Narshingdi (BK-10, 1990), and Titas (TT-11, 1990; TT-15, 2006). Samples for thin-section study were impregnated with blue epoxy to facilitate petrographic recognition of porosity. Thin sections were stained with Alizarin-Red S and potassium-hexacyanoferrate (lll) to help identify calcite and dolomite and their ferroan versions (Tucker, 1988).

The modal composition of the sandstones was achieved by counting 600 points per thin section. In the case of coarse polyminerallic rock fragments, such as quartz-feldspar granitic rock fragments, the individual mineral was counted as a single grain following the Gazzi-Dickinson point counting method (Dickinson, 1985; Dickinson and Suczek, 1979). Intergranular volume (IGV %) was determined from point-count data and is equal to the sum total of remaining intergranular porosity and the pore-filling cements and matrix.

Two scanning electron microscopes (SEM) were employed in the study: a CamScan MV 2300 SEM (University of Bonn, Germany) and a Philips XL30 tungsten filament SEM fitted with an

Oxford Instruments INCA EDS system with an SiLi detector (University of Liverpool, UK). These were used in secondary electron imaging (SEI) and backscattered electron microscope (BSEM) modes to observe authigenic minerals, cements and pore geometry in sandstones. They were also used to determine the relative timing of mineral growth and deformation. A cold Cathodoluminescence (CCL) detector was used on the Philips XL30 (University of Liverpool, UK), at 10 kV to help differentiate quartz grains and quartz cement. The SEM-CL image was built up over 16 frames.

Broken rock chips and polished sections were used for SEM examination. Broken rock chips were gold coated and examined at an acceleration voltage of 20 kV. Polished sections for BSEM and EDS analysis were coated using an Emitech K950X carbon coater. The contact between the thin section slide and sample holder was improved by painting around the sample with colloidal graphite to form a good conduction path.

Samples for X-ray diffraction (XRD) were cut from the core samples. A PANalytical X'pert pro MPD X-ray diffractometer was used for the analysis. The samples were crushed using a micromill and distilled water for 10 minutes. They were then dried overnight in a low temperature oven and powdered using agate pestle and mortar. A copper X-ray source operating at 40kV and 40mA was used. Powder samples were loaded into cavity holders and rotated continuously during the scan, completing one rotation every 2 seconds. Programmable anti-scatter slits and a fixed mask maintained in an irradiated sample area of 10 x 15 mm, with an additional 2^{o} incident beam antiscatter slit producing a flat background for raw data down to a 2theta angle of 3^{o}. The X'Celerator detector was set to scan in continuous mode with full length active pulse-height discrimination levels set to 45 to 80 %. Operation of the XRD was controlled using "HighScore Plus ®" analysis software and automated Rietveld refinement methods with reference patterns from the International Centre for Diffraction Data; Powder Diffraction File-2 Release 2008.

Doubly polished fluid inclusion wafers for fluid inclusion microthermometric studies were prepared from core samples. An Olympus BX-60 petrographic microscope, equipped with a Linkam THMSG 600 heating and cooling stage, was used for thermometry. This enabled the measurement of phase transition temperatures from -180° to 600°C with an accuracy of ± 0.1 to ± 1.0. Observations were made with different magnifications (objectives 10x, 20x, 50x and 100x). Inclusions were photographed with Digital Camera Olympus DP71 for the purpose of fast mapping of inclusion locations. Homogenization temperature measurements were made for inclusions in each small piece of fluid inclusion wafer and then freezing point depression measurements were made on each identified inclusion to prevent modification of the homogenization temperature (Worden et al., 1995). Fluid inclusion samples were also studied using a mercury UV source to differentiate oil inclusions from aqueous inclusions.

Oxygen and carbon isotope analysis from seven calcite-cemented sandstone samples of the Surma Group from the Bengal Basin (wells: JL-2, TT-11, BK-9, SN-1) (see Fig.1) was performed using a MAT 251 isotope ratio mass spectrometer. The precision was ± 0.08 ‰ for oxygen and ± 0.06 ‰ for carbon. Oxygen and carbon isotope data are presented in the δ notation relative to the Vienna Pee Dee Belemnite (VPDB) standards.

4. Results

4.1 Detrital composition and rock fabric

The Surma Group sandstones are predominantly fine-grained and moderately sorted, with minor amounts of very fine-grained and very well sorted sandstones. Grain-contacts are dominated by long, concavo-convex surfaces with some sutured contacts (Fig. 4a). Some grains have undergone brittle fracturing while others have undergone ductile compaction as shown by (Fig. 4b, c, d).

Petrographic compositions of the Surma Group sandstones is reported in Table 2. They are predominantly subarkosic to sublitharenitic in composition (Fig. 5). Intergranular volume (IGV) of the studied sandstones varies from 16 to 46.5 %. Higher values of IGV (32 – 46.5 %) have been observed in sandstones with high porosity and high cement contents (Table 2). Quartz is the most abundant detrital constituent representing 74 % of the detrital grains, on average. Monocrystalline quartz grains dominate the detrital quartz population with an average of 61 %; polycrystalline quartz are a subordinate component at 13 %. Feldspars grains represent an average of 9.9 % of the detrital grains; this is split between K-feldspar (5.0 %) and plagioclase feldspar (4.9 %). Lithic grains represent an average of 8.3 % of the detrital grains and occur as sedimentary, metamorphic and minor volcanic fragments. Metamorphic lithic grains are mainly micaceous phyllite and schist fragments. They are more abundant (5.0 %) than sedimentary lithic grains (2.6 %) which are dominated by shale fragments. Detrital phyllosilicates grains are present with almost equal amount of muscovite and biotite (averages of 3.6 % and 3.8 %, respectively). The lithic fragments are thus dominated by ductile grains. The detrital ductile grains have been deformed by plastic deformation whereas more brittle grains (e.g. quartz, feldspar grains) have undergone fracturing (Fig. 4b). Few carbonate grains and bioclasts (Fig. 4e) have been found.

4.2 Diagenetic minerals and cements

The main diagenetic minerals in the sandstones are calcite cement and clay mineral cements (chlorite, illite/illite-smectite and kaolin) with subordinate amounts of quartz and K-feldspar overgrowths (Table 2). The diagenetic constituents, in order of abundance, are: calcite, clay minerals, quartz, with only trace amounts of K-feldspar and pyrite.

4.2.1 Calcite cement

Calcite is the most abundant cement (average 6 %, maximum 37 % of the total sandstone composition). Carbonate bioclasts are present in some samples, providing possible evidence of the source of the calcite cement (Fig. 4e). Diagenetic calcite occur as: (1) microcrystalline masses (Fig. 6c), (2) coarse crystalline, poikilotopic, pore-filling masses (Fig. 6d), (3) isolated rhombs (Fig. 6e), (4) partial grain replacements (e.g. within altered feldspar or lithic grains) (Fig. 6f). Poikilotopic calcite (forming an interlocking mosaic of crystals) locally replaces detrital quartz, feldspar, micas and clay-rich ductile grains. Ferroan calcite is the dominant cement in these sandstones. Poikilotopic calcite cement preserves an intergranular volume (IGV) of up to 41 % and fills relatively large pores between loosely packed framework grains. This type of calcite does not fill fractures or extend into partially corroded grains. Pore-filling calcite cement in these sandstones is locally associated with secondary pores in plagioclase.

4.2.2 Clay mineral cements

Clay minerals represent an average of 4.6 % and include chlorite, illite, illite-smectite and kaolinite, as revealed by thin section petrography, SEM and XRD (Fig. 7a). In the clay fractions of these sandstones, XRD spectra indicate an overall relative chlorite content of up to 22 %, a combined illite and smectite content up to 53 %, and a kaolinite content of up to 25 %.

Authigenic chlorite can be observed throughout the collection of samples. Chlorite contents ranging from trace to 5.7 % (average 1.3 %). Detrital biotite has been locally replaced by chlorite (Fig. 4a). Secondary X-ray analysis in the SEM X revealed that the chlorite is iron-rich (Fig. 7b). Grain-coating clay minerals, dominated by chlorite, are locally found around detrital grain surfaces in these sandstones (Fig. 6a, b). The chlorite rims (Fig. 8a) are generally discontinuous. Chlorite consists of small irregular to pseudo hexagonal platelets, 2-3 μm in length, aligned in a grain-perpendicular form. Chlorite rims are locally enclosed by quartz overgrowths (Fig. 8b).

Fibrous illite is not abundant in these sandstones, but illite/smectite mixed layer clays are common with lath-like and crenulated morphology with honeycomb-like crystals (Fig. 8c, d).

Illite-smectite locally occurs as a grain coating (pore-lining) and pore-filling clay as well as occurring as a replacement product of detrital micas.

Kaolinite is found in primary pore spaces as stacks of booklets, vermiform aggregates (Fig. 8a), within altered mica grains, as well as in close association with secondary pores in feldspar grains (Fig. 8d). Kaolinite is also present as blocky euhedral, pseudohexagonal plates sitting in primary pores and has been locally altered to dickite, the high temperature kaolin polymorph (Fig. 8e, f)

4.2.3 Quartz and feldspar cements

Quartz cement is routinely observed but represents a relatively minor component in these sandstone reservoirs, ranging from trace quantities to as much as 6.2 %, with an average of 2.3 %. It is present as quartz overgrowths around detrital quartz grains (Fig. 9a-d). In some cases, the boundaries between quartz grains and the quartz overgrowths are marked by clay mineral coatings and dust lines (Fig. 9a). Some examples of complete, grain-rimming quartz overgrowths are present (Fig. 9c, d) although in most cases quartz cement occurs as small (10-20 μm) isolated, euhedral outgrowths on detrital quartz grains. In some cases, quartz overgrowth development was inhibited by localized chlorite grain coats (Fig. 8b). Well-established euhedral quartz overgrowths are found only where chlorite grain coats are absent or rare. Most quartz overgrowths are inclusion-free or contain inclusions that are too small to use for microthermometry (< 5 μm). However a few aqueous inclusions were large enough to be used for microthermometry yielding last-ice melting temperatures, T_m, of -1.8 to -7.8°C and homogenization temperatures, T_h, of 113 to 150°C. No fluorescent petroleum inclusions were found.

Minor feldspar overgrowths have been found on detrital plagioclase. Plagioclase grains have also been partially albitized (Fig. 9e).

4.2.4 Pyrite cement

Pyrite cement is present as framboidal aggregates as revealed by SEM (Fig. 9f). Pyrite sits within the intergranular pores surrounded by illite/smectite mixed layer clay coated detrital grains.

4.3 Stable isotope results

Isotopic data from poikilotopic calcite cement are presented in Table 2. $\delta^{18}O$ values range between –11.7‰ and –6.9 VPDB. Calcite $\delta^{13}C$ values sit within a range from –18.2‰ to –4.1 to VPDB. Slightly more negative $\delta^{13}C$ values have been previously reported (Rahman and McCann, 2012) from the northeastern part of Bengal Basin (Surma Basin, Fig. 10).

4.4 Porosity and Permeability

Core analysis porosity ranges from 3 to 28 %; core analysis permeability ranges from 0.15 to 1,230 mD (BAPEX, 1996; Islam, 2010).

Petrographic microscopy and SEM analysis showed that the sandstones exhibit three different types of porosity: (i) intergranular macroporosity (primary porosity), (ii) secondary porosity and (iii) microporosity associated with clay minerals, that is probably secondary in origin (Fig. 8a-f).

The total porosity (primary and secondary) comprises an average 18 % of the rock volume (ranging from 0 to 31 %). Sandstones with high ductile grain contents tend to have lower porosity than those with low ductile grain contents (Fig. 11). Petrographically-defined total porosity tends to decrease with increasing depth of burial with the lowest porosities found at depths > 3000 m (Fig. 11).

Petrographically-defined primary porosity has an average value of 14 %, ranging from 0 to 27 %. Secondary porosity has an average of about 4 %, ranging from 0 to 11 %. The development of the majority of the secondary porosity occurred due to the dissolution of detrital feldspar grains

(Fig. 6a, b) and carbonate grains (Fig. 4a) and cement (Fig. 4c); most secondary porosity is ineffective since it is filled with authigenic clay. Dissolution resulted in mouldic, oversized secondary pores (bigger than primary pores) in some samples, with the secondary pores outlined by clay mineral rims (Fig. 6b). Dissolution locally enhanced the porosity of the reservoir. However, the secondary pores are associated with clay minerals, so the permeability is unlikely to have been improved by dissolution processes.

Point count thin section porosities (0 to 31 %) are overall in good agreement with those of the core plug porosities, although thin section porosity is, in most cases, lower than the core plug porosity, which indicates the presence of microporosity. Low angle cross-bedded, clean sandstones have the highest porosity and permeability values. Twenty percent porosity can lead to permeability ranging from 10 mD up to several hundred mD (Fig. 12). Variation of detrital ductile grain proportions, calcite cement content, clay mineral content and quartz cement have resulted in the wide range of permeability for sandstones of a given porosity.

Intergranular volumes for the 86 point counted samples are highly variable (ranging from 16 to 46.5 %). Sandstones with primary porosities ≥20 % have average IGV values of 35 %. The intergranular volume of microcalcite cemented samples is up to 32 % (Fig. 6c) while poikilotopic calcite cement preserves an intergranular volume of up to 41 %.

5. Discussion

5.1 Sequence of diagenetic events

The presence of framboidal pyrite (Fig. 9f) requires near-surface, low temperature, sulphate reducing bacteria in the presence of sulphate-rich marine pore waters (Berner, 1980); pyrite was probably one of the first minerals to grow in these sandstones, confirming the marine influence on these sandstones.

Grain-contacts are dominated by long, concavo-convex surfaces with some suture contacts. This suggests that the sandstones might have been subjected to moderate to high degree of mechanical compaction. Whereas simple grain reorganization was probably the first, and possibly dominant, form of mechanical compaction, as shown by large scale studies of compaction from other basins (Paxton et al., 2002), there have also been other types of mechanical compaction. These include ductile (plastic) deformation of lithic fragments (Fig. 4b, c) and the brittle fracturing of quartz and feldspar grains (Fig. 4b) indicating both ductile and brittle grain compaction in these sandstones.

Grains coated with clays (Fig. 6a, b) may have developed immediately after deposition due to mechanical infiltration at sites where the sediment was exposed at the surface (Matlack et al., 1989; Moraes and De Ros, 1990, 1992) or by bioturbation processes (McIlroy et al., 2003; Needham et al., 2005; Worden et al., 2006). Authigenic chlorite is significant because, studies from other basins have shown that, it can create continuous grain coatings that inhibit quartz cement growth (Bloch et al., 2002). Chlorite typically develops at temperatures of > 60 or 70ºC (Worden and Morad, 2003). In these sandstones, authigenic chlorite is associated with biotite-rich sandstones (Fig. 4a). Chlorite in the Surma Group may have formed by: (1) the diagenetic replacement of detrital biotite (Fig. 4a), or (2) the transformation of precursor infiltrated or grain-coating clay minerals (Figs. 6e, 8a), or by a combination of these two processes.

Since diagenetic calcite in the Surma Group sandstones occur in a variety of forms (Fig. 6c-f), it is likely that the growth of calcite occurred over a range of diagenetic temperatures. Poikilotopic calcite cement preserves an intergranular volume (IGV) of up to 41 % and fills relatively large pores between loosely packed framework grains, it is here interpreted to have formed very early in the burial history before significant compactional porosity-loss could occur. Microcrystalline calcite appears to have developed somewhat later, during or after mechanical compaction, since the intergranular volume of microcrystalline calcite cemented samples is up to 32 % (Fig. 6c).

The presence of grain coating illite, with hair-like and honeycomb-like crystals with spiny terminations, indicates a diagenetic origin, as opposed to detrital origin (Lemon and Cubitt, 2003; Morad et al., 2000). Illite typically forms during progressive burial (mesodiagenesis) at temperatures > 90°C through the transformation of depositional or infiltrated clays (e.g. smectite conversion to illite via mixed layer illite-smectite) (Keller et al., 1986; Morad et al., 2000). Illitization of smectite requires a source of potassium, in this case probably supplied from the alteration of feldspars (Ehrenberg, 1993; Morad and De Ros, 1994; Morad et al., 2000). By inference, the alteration of feldspar, generation of illite and creation of secondary pores (Fig. 6a, b) may have been coincident.

Kaolinite is closely associated with decomposed feldspar grains and, thus probably formed by the alteration of detrital feldspar grains (Fig. 8d). The creation of kaolinite requires feldspar either in low salinity or low pH (acidic) formation water. Acidic pore waters could plausibly have been generated at depth during the maturation of organic matter in adjacent shale (Rahman and McCann, 2012). The growth of carbonate minerals due to an influx of CO_2 (e.g. from source rocks) has been associated with the concomitant alteration of feldspar to kaolinite due to the acid buffering by the feldspar-clay reaction (Barclay and Worden, 2000; Worden and Barclay, 2000). The presence of blocky dickite associated with kaolinite in the deeper samples (Fig. 8e-f) has been previously explained as a function of polymorphic transformation as a function of temperature (Beaufort et al., 1998).

The presence of quartz cement as a syntaxial overgrowth near the sites of intergranular dissolution, and around tightly packed detrital quartz grains, indicates a mesogenetic origin (McBride, 1989; Worden and Morad, 2000). Fluid inclusion homogenization temperatures range from 113 to 150ºC suggesting a relatively late onset of quartz cement, most likely due to the limited time available at these high temperatures for these Miocene sandstones (Walderhaug et al., 2000). The numerous long intergranular concavo-convex contacts between individual quartz grains and some suture contacts (Fig. 4a) seem to suggest that *in situ* pressure solution at stylolites may account for some of the quartz cement present. Alternative internal sources of silica may have been effective as well as, or instead of, stylolites; these include the conversion of K-feldspar to clay minerals (Worden and Morad, 2000) and the progressive transformation of smectite to illite (McKinley et al., 2003).

An overall paragenetic sequence of the dominant diagenetic features of the Bhuban Formation (Surma Group) sandstones from the Bengal Basin is presented in Figure 13. This interpreted sequence of events is based on the mutual textural relationship of thin section and SEM observations described and interpreted in the previous sections (Figs. 4, 6, 8-9).

5.2 Conditions during calcite growth

An intergranular volume of 41 % for poikilotopic calcite-cemented sandstones implies that calcite growth occurred before mechanical compaction strongly affected primary depositional porosity, requiring that poikilotopic calcite grew at low temperature. An oxygen isotope value of –9.3 ‰ (± 2.4 ‰) from poikilotopic calcite cements has been used in conjunction with the calcite-water oxygen isotope fractionation equation (Friedman and O'Neil, 1977) to reveal the conditions during calcite diagenesis. If we assume poikilotopic calcite grew at 30°C then water with a $\delta^{18}O$ value of about –6 ‰ VSMOW must have been present (with a range from -4 to -9 ‰). Alternatively, if we assume that seawater with a $\delta^{18}O$ value of 0 ‰ VSMOW was responsible for poikilotopic calcite, then it would have grown at a temperature of 71°C (with a range from 55 to nearly 100°C) (Fig. 14); such high temperatures are untenable for calcite growth given the high IGVs. On this basis it may be concluded that meteoric pore waters were present during poikilotopic calcite growth (Figs. 13 and 14).

5.3 Depositional controls on diagenesis and reservoir quality

Reservoir quality of the Surma Group has been strongly influenced by depositional environment as well as various types of diagenetic alteration. In the analyzed samples, clean sandstones that are massive or have low angle cross-bedding have the best reservoir quality since they have the highest detrital quartz content, lowest matrix content and to be fine to medium grain-size and well sorted. Of the three representative sub-environments identified, high energy distributary channel sediments have the highest grain size and thus had the best primary reservoir quality characteristics. In contrast, shore face sandstones are very fine to medium grained and thus had the worst primary reservoir quality characteristics. The lower energy, tidal flat sandstones are fine-grained sandstones and had intermediate primary reservoir quality characteristics. The presence of depositional mud-flakes and clay drapes decreased permeability during burial owing to their exacerbated mechanical compaction and the formation of pseudo-matrix (Fig. 4d). Where the depositional matrix content is elevated, there is locally reduced porosity in the reservoir (Sample TT-11 (18), TT-11 (27) Table 2).

5.4 Diagenetic controls on reservoir quality

5.4.1 Mechanical compactional controls on reservoir quality

Mechanical compaction is a collection of processes that lead to volume-reduction due to applied effective stress. Mechanical compaction occurs progressively during burial. It theoretically occurs in a variety of ways including the simple process of grain reorganization changing a sediment’s fabric from loose random packing at deposition to hexagonal close-packing following burial to >2,000m. This diminishes porosity from an initial 45 % to a post-grain repacking value of 26 % (Paxton et al., 2002). Mechanical compaction also operates by grain bending, ductile deformation of mechanically-weak grains (Fig. 4b, c) and fracturing of brittle but weak minerals (Fig. 4b). The specific effects of mechanical compaction during burial can be seen by comparing porosity to depth with the data subdivided by petrographically-defined ductile grain content (Fig. 11). This diagram has been overlaid with model mechanical compaction curves for different ductile grain content (Ramm et al., 1997; Worden et al., 2000). Significant overpressure has not ben reported for these sandstones so we have not attempted to factor in over-pressure inhibited compaction and porosity-preservation in this analysis (Osborne and Swarbrick, 1999; Ramm and Bjorlykke, 1994). The lowest porosities are found in sandstones with the highest ductile grain contents (Fig. 11) suggesting that ductile compaction has been important within Surma Group sandstones. For the depth of burial, the reported porosity for most samples is significantly lower than it would have been if only mechanical compaction had occurred suggesting that there has been an additional process responsible for porosity-loss in these sandstones.

The role of mechanical compaction on porosity and permeability can also be discerned from Figure 12: the shallowest, and thus lowest effective stress, samples have the highest porosity and permeability. Also, the sandstones with the higher ductile contents tend to have lower permeability for a given porosity than those with lower ductile contents. The paramount role of ductile grains in Miocene sandstones reservoirs in SE Asia has been noted previously (Worden et al., 2000).

Whether mechanical compaction or cementation has been the dominant control on porosity can be determined by evaluating IGV, cement content and porosity and creating a Houseknecht diagram (Fig. 15) (Houseknecht, 1987). This diagram shows that mechanical compaction is the dominant control on porosity-loss in most sandstones. Mechanical compaction has generally exerted a bigger control on porosity than growth of cements. The exceptions are the sandstones that contain large quantities of calcite cement in which compactional porosity-loss was not possible. Sandstones with greater initial proportions of ductile grains tend to have the greatest degree of compactional porosity-loss (Fig. 15), thus confirming the significance of ductile grains deduced from the porosity-permeability plot (Fig. 12).

5.4.2 Diagenetic cement controls on reservoir quality

The growth of pore-filling cements explains why porosity values are lower than they would be had only mechanical compaction occurred. Poikilotopic calcite cement has locally reduced porosity down to 3 to 7 % and permeability down to < 0.15 mD in some samples (Figs. 13, 16a, b). The $\delta^{13}C$ VPDB values from calcite cement from the Bengal Basin range between from −18.2 to −4.1 ‰ VPDB (Fig. 10; Table 2). This range is extended to −23.1 ‰ to 1.4 ‰ by reference to previous work (Rahman and McCann, 2012). Strongly negative $\delta^{13}C$ values require an organic source of carbonate while values close to 0 ‰ suggest that there may have been a marine bioclastic source of carbonate (Morad, 1998). Petrographic evidence of bioclasts (Fig. 4e) confirms that values close to 0‰ are the result of bioclastic debris supplying some of the calcite. However, the prevalence of strongly negative calcite $\delta^{13}C$ values suggests that much carbonate was derived from the breakdown of organic matter supplied as CO_2, possibly from early source rock maturation or resulting from biogenic sources during intermediate burial (Irwin et al., 1977). Organic sources of CO_2 still require a source of calcium to allow calcite to grow. Since pore-filling calcite cement is locally associated with secondary pores in plagioclase (Fig. 6f), this leads to the conclusion that calcic-feldspar breakdown may be at least partly responsible for calcite growth. Petroleum systems are typically flooded with source rock-derived CO_2 before the main phase of oil generation and the CO_2 may also have induced alteration of the feldspars by dissociation in water leading to carbonic acid formation (Barclay and Worden, 2000; Worden and Barclay, 2000). We have not detected a role for oil emplacement on calcite cement abundance: i.e we have not found any evidence of inhibition of calcite cement due to the emplacement of oil (De Souza and Silva, 1998). This may be due to the fact that calcite grew early either due to bioclast dissolution (Fig. 4f) or due to a pre-oil emplacement flux of source-rock derived CO2 (Fig. 10).

Clay minerals represent the second most volumetrically significant group of pore-filling cements that affect porosity and permeability (Figs. 8, 16c and d). Pore-filling illite-smectite (Figs. 7 and 8c) slightly reduces porosity, but based on precedents from other basins, has a dramatic effect on permeability (McKinley et al., 2003; Worden and Morad, 2003). Authigenic kaolinite locally occludes pore spaces although much of it seems to have replaced feldspars and has resulted in redistributional secondary micro-porosity (Giles and Deboer, 1990) (Figs. 7 and 8a, f, e). The poikilotopic calcite oxygen and carbon isotope data have been interpreted to suggest that meteoric water influx combined with organic-derived CO_2 were important during diagenesis (Figs. 10 and 14). An influx of low salinity water and CO_2 are conducive to the conversion of feldspars to clay minerals cation-rich smectite into higher temperature clays such as kaolinite and illite. Thus the conditions that resulted in poikilotopic calcite growth may also have led to silicate diagenetic reactions. The silicate reactions act as a pH buffer for the hydrogen ions that result from CO_2 dissolution and dissociation followed by calcite precipitation:

CO_2 dissolution and dissociation: $CO_2 + H_2O \Leftrightarrow HCO_3^- + H^+$ (R1)

Calcite precipitation: $HCO_3^- + Ca^{2+} \Leftrightarrow CaCO_3 + H^+$ (R2)

K-feldspar alteration to illite: $3KAlSi_3O_8 + 2H^+ \Leftrightarrow KAl_3Si_3O_{10}(OH)_2 + 2K^+ + 6SiO_2$ (R3)

Plagioclase alteration to kaolinite: $CaAl_2Si_2O_8 + 2H^+ \Leftrightarrow Al_2Si_2O_5(OH)_2 + Ca^{+2+}$ (R4)

Both of the feldspar replacement reactions (R3 and R4) buffer the pH (use up hydrogen ions) and allow reactions R1 and R2 to continue. Thus feldspar alteration, clay growth and carbonate growth may all be genetically connected.

Small amounts of quartz cement (average of 2.3%) have been found in the Surma Group (Figs. 9a - d) showing that quartz cement has played only a minor role in reducing porosity and permeability. The relatively small volume of quartz cement in these sandstones can be attributed to a number of factors: (i) the limited amount of time spent above the critical onset temperature of 80°C (Walderhaug et al., 2000), (2) the presence of grain coating clay (Dowey et al., 2012; Worden and Morad, 2003) and possibly (3) the limited amount of residual water in these gas-charged sandstones that is available to facilitate water-rock interaction (Worden et al., 1998). There is an inverse relationship between the amount of chlorite and the amount of authigenic quartz (Figs. 8b, 17). Chlorite grain coats may therefore have inhibited quartz cement and helped to preserve porosity, a phenomenon that has been reported in many basins around the world (Dowey et al., 2012).

5.5 Comparison of the Surma Group to other Miocene sandstones at 2,300 to 3,200m

Miocene sandstones at buried to greater 2,000 m have been assessed for reservoir quality and diagenesis in several petroliferous basins around the world including those in SE Asia, Gulf of Mexico, Central Europe and California. They have several features in common that result from the rapid accumulation of sediment.

Mechanical compactional processes, especially ductile compaction, play a paramount role in controlling reservoir quality in many Miocene reservoirs, as well as the Surma Group sandstones discussed here. The rapid supply of mineralogically immature sediment, with an innate tendency to undergo ductile compaction, is important for Miocene sediments in parts of the Gulf of Mexico (Dutton et al., 2012), SE Asia (Worden et al., 2000) and Central Europe (Gier et al., 2008). The high rate of Miocene sediment accumulation, e.g. ten times that responsible for the accumulation and burial of the Brent Group in the North Sea, (Giles et al., 1992), suggests that there will have been limited time for the supplied sediment to become cleaned-up during transport from the hinterland to the site of final accumulation.

Similar to the Surma Group sandstones in the Bengal Basin, the important role of calcite cement, with a lesser role or dolomite cement, is a common to most Miocene sandstones in SE Asia, Gulf of Mexico, Central Europe and California (Ali, 1995; Boles and Ramseyer, 1987; Dutton et al., 2012; Fayek et al., 2001; Gier et al., 2008). Where isotope studies have been undertaken (Ali, 1995; Fayek et al., 2001), the carbonate cements were, like the Surma Group calcite cements, interpreted to be a result of a combination of marine (presumably bioclastic) sources and various organic sources.

Alteration of plagioclase grains is endemic to Miocene sandstones, and not just those in the Surma Group (Boles and Ramseyer, 1987; Dutton et al., 2012; Gier et al., 2008; Hirt et al., 1993). Also similar to the Surma Group, clay minerals in these sandstones typically represent a collection of depositional (smectite-illite) and early diagenetic (kaolinite) clays that have yet to achieve the illite-dominated characteristics typical of older sandstones at about 3,000m (and >100°C) burial

Quartz cement is routinely present in Miocene sediments buried to the 2,300 to 3,200 m (85 to 115°C) found in the Surma Group sandstones in this study, but it is usually present in smaller amounts than would be expected in Mesozoic sandstones at this depth (temperature) range. Compared to the Surma Group sandstones, quartz cement was found in similar quantities in Miocene sandstones at similar depths in Central Europe (Gier et al., 2008) and SE Asia (Worden et al., 2000). At significantly greater depths of burial (and higher temperatures), rather more quartz cement is typically found in Miocene sandstones (Dutton et al., 2012; Worden et al., 2000) although porosity is typically higher than might be expected than for Mesozoic sandstones. The lack of quartz cement at >100°C in Miocene sandstones has been attributed to the lack of time available to grow quartz cement (Gier et al., 2008).

6. Conclusions

1) The Miocene Surma Group in the Bengal Basin, buried to 2300 m and 3200 m, contains sub-arkosic to sub-litharenitic, tide-dominated, deltaic sandstones.
2) The main reservoir quality control in these young, but relatively deeply buried, sandstones is mechanical compaction. Depth of burial and the detrital ductile grain content had important controls on the extent of mechanical compaction. Lithic ductile-rich sandstones have undergone more compaction than ductile-poor sandstones.
3) Cement growth was less important than mechanical compaction in these sandstones, but poikilotopic calcite is the main diagenetic cement. This calcite grew (or dissolved and then reprecipitated) in meteoric water at relatively low temperature . Calcite cement was derived from a combination of marine bioclastic grains and organic CO_2 sources, such as biogenic breakdown or early thermal maturation.
4) Partly illitized smectite occurs in these sandstones and, where present, it locally blocks pore throats. Small amounts of kaolinite occurs as a partial replacement of feldspar grains. Fe-rich chlorite locally coats sand grains.
5) Quartz cement is not particularly important in these Miocene sandstones even though burial temperatures have reached >100°C; this is probably due to a combination of the limited time at elevated temperatures and the presence of grain-coating chlorite.
6) Reservoir quality in the Miocene Surma Group sandstones is predominantly limited by sediment supply (controlling ductile grain and clay mineral contents), depositional environment (influencing bioclast and clay mineral contents) and burial history (largely controlling the thermal stress).

7) Good reservoir quality sandstones, with high porosities (20 % to 30 %) and permeabilities (34 to 1230 mD), have been observed at a range of depths (2300 m and 3200 m in Surma Group sandstones in the Bengal Basin. The best reservoir quality sandstones are fine to medium grained and show good sorting, have a low primary ductile grain content and a small amount of calcite cement (i.e. low primary bioclasts content).
8) Good reservoir quality sandstones are not uniformly distributed and instead are locally compartmentalized by poorly sorted and tightly compacted, ductile-rich sandstones, and sandstones with extensive cementation (poikilotopic calcite in particular) having porosity (3 - 7 %) and permeability (0.15 – 1.4mD).

Acknowledgements

First author would like to thank Commonwealth Scholarship Commission (CSC) United Kingdom for granting a Commonwealth Academic Fellowship (2012) to carry out this research project. This work was partly sponsored by Alexander von Humboldt Foundation (AvH), Germany. We are grateful to BAPEX (Bangladesh Petroleum Exploration and Production Company) for giving permission to analyze core samples. We are thankful to Prof. Dr. Andreas Mackensen, Alfred Wegener Institute, Germany and Dr Steve Crowley, stable isotope laboratory of Earth and Ocean Sciences of University of Liverpool, UK for isotope analysis.

Figure captions

Figure 1. Major tectonic elements of the Bengal Basin (Alam et al., 2003; Alam and Curray, 2003) and locations of the petroleum exploration wells: BK-9 (Bakhrabad-9-Meghna Gas Field) BK-10 (Bakhrabad-10-Narshingdi Gas Field), JL-Jalalabad, SN-SaldaNadi, TT-11 (Titas-11 of the Titas Gas Field), TT-15 (Titas-15 of the Titas Gas Field)

Figure 2. Lithofacies of the Surma Group (SG) encountered in BK-9 (Meghna), BK-10 (Narshingdi), TT-11 (Titas-11) and TT-15 (Titas-15) wells. •sample location

Figure 3. Burial history diagrams of: (a) Bakhrabad area (BAPEX, 1996) where BK-9 (Bakhrabad-9 of the Meghna Gas Field) and BK-10 (Bakhrabad-10 of the Narshingdi Gas Field) wells are situated; (b) Titas Gas Field (Islam, 2009), in the Bengal Basin.

Figure 4. a. Photomicrograph showing long intergranular concavo-convex contacts between individual quartz grains and some suture contacts (sc), biotite (b) being altered to chlorite, partly dissolved carbonate grain (c) and feldspar (F), depth 2698.4 m, well TT-11 (Titas); b. BSE image showing brittle- and ductile-grain compaction, depth 2473 m, well JL-3 (Jalalabad-3); c. deformed ductile grain (mica) occluding pore space and isolating remaining pore space as it extruded between rigid grains, depth 2307.9 m, well BK-9 (Meghna); d. Pseudomatrix (Pm) formed due to mechanical compaction of clay clasts; e. Bioclast contributing carbonate cement generation, depth 2709.4 m, well TT-11 (Titas)

Figure 5. Modal composition and classification of the Surma Group sandstones in the Bengal Basin. The fields are from McBride (1963). For symbol explanation, see Figure 1.

Figure 6. Photomicrographs of sandstones showing: (a) Infiltrated clay minerals (Cl), partial to almost completely dissolved plagioclase resulting secondary porosity (SP), BK-9 well (Meghna) at depths 2308.5 and 2317.7 m; (b) mouldic secondary porosity (SP) with clay-

mineral rim -depth 2597 m, JL-2 (Jalalabad); (c) BSE image showing poikilotopic pore-filling intermediate calcite-depth 2789.9 m, well TT-11 (Titas); (d) Photomicrographs showing Poikilotopic pore-filling early calcite cement (Fe-C, Fe-calcite) - depth 2307 m, well BK-9 -2 (Meghna); (e) BSE image of isolated pore-filling late carbonate cement, depth 2659 m, well JL-2 (Jalalabad); (f) Isolate late carbonate cement associated with plagioclase dissolution (Pg-C)- depth 2588 m, well JL-2 (Jalalabad).

Figure 7. (a) XRD spectra (glycolated) of clay separate of sandstone at depth 2597 m, Jalalabad. (b) Characteristic energy dispersive secondary X-ray spectra of chlorite.

Figure 8. Scanning electron micrographs of sandstones showing: (a) BSE image of microporous vermiform kaolinite aggregates (K), thin chlorite rim (Ch), grain coating chlorite (gc-ch) depth 2608 m, well Jalalabad-2; (b) Platelets of authigenic chlorite (Ch) that retards quartz overgrowth (QO), depth 2307.9 m, well BK-9 (Meghna); (c) Pore filling Illite-smectite (Ill-sm), depth 2923.3 m, well BK-10 (Narshingdi); (d) BSE image of pore filling illite-smectite (Ill-sm), kaolinite (K) and dissolved feldspar (F), depth 2603 m, well JL-2 (Jalalabad); (e) Pore-filling kaolinite (kaolinite, K, dickite, D; depth 3175.1 m, well BK-10 (Narshingdi); (f) enlarged view of pore-filling kaolinite in Fig. 8e.

Figure 9. (a) Photomicrograph of sandstone showing quartz overgrowth occluding pore throats, depth 2588 m, well JL-2 (Jalalabad); (b to d) Scanning electron micrographs of sandstones showing: b. SEM-CL image of quartz cement partially narrowing pore throat, depth 2608 m, well JL-2 (Jalalabad); c. Interlocking quartz cement (QO) reducing pore throat), depth 2989.9 m, well TT-11 (Titas); d. Well developed quartz overgrowth (QO) hindering chlorite (Ch) development, depth 3131.3 m, well TT-15 (Titas); e. BSE image showing feldspar overgrowth on plagioclase, depth 2659 m, well JL-2 (Jalalabad); f. Framboidal aggregates of pyrite, depth 3135 m, well TT-15 (Titas-15).

Figure 10. $\delta^{18}O$ versus $\delta^{13}C$ for calcite of the Surma Group sandstones, Bengal Basin. Data from Rahman and McCann (2012) are from northeastern Bengal Basin (Fig. 1). Low $\delta^{18}O$ values typically represent growth at high temperatures. Low $\delta^{13}C$ values represent little bioclastic input influencing the carbonate, but more kerogen-derived CO_2.

Figure 11. Porosity (point counted, %) versus depth and ductile grain contents compared to modelled mechanical compaction curves (Worden et al., 2000; Worden et al., 1997).

Figure 12. Core porosity vs. core permeability of the Surma Group sandstones, Bengal Basin. Data have been split by detrital ductile content and into shallow (<2700m) and deep (>2700m) samples.

Figure 13. Paragenetic sequences for the sandstone of the Surma Group.

Figure 14 Cross plot of derived formation water $\delta^{18}O$ versus temperature for a range of poikilotopic calcite $\delta^{18}O$ values using the calcite-water oxygen isotope fractionation equation in Friedman and O'Neill (1977). The mean calcite $\delta^{18}O$ value is -9.3‰ VPDB with a maximum of -6.9‰ and a minimum of -11.7‰. If we assume that the calcite grew at low temperature (~30°C), before mechanical compaction reduced the IGV to less than 41%, then the water from which calcite grew must have had a relatively low $\delta^{18}O$ value typical of meteoric water (between -4 and -9‰ VSMOW, with a mean of -7‰). If seawater had been responsible for calcite growth, this could only have occurred at a temperature of approximately 71°C (with a range from 55 to 100°C); such temperatures are incompatible with the high IGV values.

Figure 15. Intergranular volume (%) versus cement (%). Diagram after (Houseknecht, 1987).

Figure 16. Core porosity-permeability controls: (a) Porosity versus calcite cement, (b) Permeability versus calcite cement, (c) Porosity versus clay mineral cement, (d) Permeability versus clay mineral cement, (e) Porosity versus quartz cement, (f) Permeability versus quartz cement.

Figure 17. Relationship between petrographically-determined authigenic chlorite and quartz cement split be present day (maximum) depth of burial. Quartz cement is only present at > 4 % when chlorite is present at < 2 %. The maximum amount of quartz cement increases in more deeply buried (i.e. hotter) samples.

Table caption

Table 1 Stratigraphic succession of the Bengal Basin (after Rahman and McCann, 2012).

Table 2 Petrographic and stable-isotope composition, as well as porosity-permeability values for the 85 analysed sandstone samples encountered in seven petroleum exploration wells (JL-2-Jalalabad 2, JL-3-Jalalabad 3, BK-9-Bakhrabad 9, BK-10-Bakhrabad 10, SN-1). The Gazzi-Dickinson method was used for point counting (Dickinson, 1985; Dickinson and Suczek, 1979). Only calcite-cement content and isotope values are given for sandstone of the Salda Nadi well. IGV: intergranular volume

References

Alam, M., 1989. Geology and depositional history of Cenozoic sediments of the Bengal Basin, Bangladesh. Palaeogeography Palaeoclimatology Palaeoecology 69, 125-139.

Alam, M., Alam, M.M., Curray, J.R., Chowdhury, A.L.R., Gani, M.R., 2003. An overview of the sedimentary geology of the Bengal Basin in relation to the regional tectonic framework and basin-fill history. Sedimentary Geology 155, 179-208.

Alam, M.M., 1995. Tide-dominated sedimentation in the Upper Tertiary succession of the Sitapahar Anticline, Bangladesh, in: Flemming, C.G., Bortholma, A. (Eds.), Tidal signatures in modern and ancient sediments. International Association of Sedimentologists, Special Publication. Blackwells, Oxford, pp. 329-341.

Alam, M.M., Curray, J.R., 2003. The curtain goes up on a sedimentary basin in south-central Asia: unveiling the sedimentary geology of the Bengal Basin of Bangladesh - Special Issue. Sedimentary Geology 155, 175-178.

Ali, M.Y., 1995. Carbonate cement stratigraphy and timing of diagenesis in a Miocene mixed carbonate-clastic sequence, offshore Sabah, Malaysia - constraints from catholuminescence, geochemistry, and isotope studies. Sedimentary Geology 99, 191-214.

BAPEX, 1996. Petroleum geology of Bangladesh, Core Laboratory Report. Bangladesh Petroleum Exploration & Production Co. Ltd, Dhaka, p. 139.

Barclay, S.A., Worden, R.H., 2000. Geochemical modelling of diagenetic reactions in a sub-arkosic sandstone. Clay Minerals 35, 57-67.

Beaufort, D., Cassagnabere, A., Petit, S., Lanson, B., Berger, G., Lacharpagne, J.C., Johansen, H., 1998. Kaolinite-to-dickite reaction in sandstone reservoirs. Clay Minerals 33, 297-316.

Berner, R.A., 1980. Early diagenesis, a theoretical approach. Princeton University Press, Princeton.

Bloch, S., Lander, R.H., Bonnell, L., 2002. Anomalously high porosity and permeability in deeply buried sandstone reservoirs: Origin and predictability. American Association of Petroleum Geologists Bulletin 86, 301-328.

Boles, J.R., Ramseyer, K., 1987. Diagenetic carbonate in Miocene sandstone reservoir, San Joaquin basin, California. American Association of Petroleum Geologists Bulletin 71, 1475-1487.

De Souza, R.S., Silva, D.A., 1998. Origin and timing of carbonate cementation of the Namorado Sandstones (Cretaceous), Albacora Field Brazil: implication for oil recovery. In: Carbonate cementation in sandstones (ed. Morad, S.) International Association of Sedimentologists Special Publications 26, 309-325.

Dickinson, W.R., 1985. Interpreting provenance relation from detrital modes of sandstones, in: Zuffa, G.G. (Ed.), Provenance of Arenites: NATO ASI Series, C 148. D. Reidel Publishing Company, Dordrecht, pp. 333-363.

Dickinson, W.R., Suczek, C.A., 1979. Plate tectonics and sandstone compositions. American Association of Petroleum Geologists Bulletin 63, 2164-2182.

Dowey, P.J., Hodgson, D.M., Worden, R.H., 2012. Pre-requisites, processes, and prediction of chlorite grain coatings in petroleum reservoirs: A review of subsurface examples. Marine and Petroleum Geology 32, 63-75.

Dutton, S.P., Loucks, R.G., Day-Stirrat, R.J., 2012. Impact of regional variation in detrital mineral composition on reservoir quality in deep to ultradeep lower Miocene sandstones, western Gulf of Mexico. Marine and Petroleum Geology 35, 139-153.

Ehrenberg, S.N., 1993. Preservation of anomalously high-porosity in deeply buried sandstones by grain coating chlorite - examples from the Norwegian continental shelf. American Association of Petroleum Geologists Bulletin 77, 1260-1286.

Fayek, M., Harrison, T.M., Grove, M., McKeegan, K.D., Coath, C.D., Boles, J.R., 2001. In situ stable isotopic evidence for protracted and complex carbonate cementation in a petroleum reservoir, North Coles Levee, San Joaquin Basin, California, USA. Journal of Sedimentary Research 71, 444-458.

Friedman, I., O'Neil, J.R., 1977. Compilation of stable isotope fractionation factors of geochemical interest. US Geological Survey Professional papers.

Gibbons, A.D., Whittaker, J.M., Muller, R.D., 2013. The breakup of East Gondwana: Assimilating constraints from Cretaceous ocean basins around India into a best-fit tectonic model. Journal of Geophysical Research-Solid Earth 118, 808-822.

Gier, S., Worden, R.H., Johns, W.D., Kurzweil, H., 2008. Diagenesis and reservoir quality of Miocene sandstones in the Vienna Basin, Austria. Marine and Petroleum Geology 25, 681-695.

Giles, M.R., Deboer, R.B., 1990. Origin and significance of redistributional secondary porosity. Marine and Petroleum Geology 7, 378-397.

Giles, M.R., Stevenson, S., Martin, S.V., Cannon, S.J.C., Hamilton, P.J., Marshall, J.D., Samways, G.M., 1992. The reservoir properties and diagenesis of the Brent Group: a regional perspective, in: Morton, A.C., Haszeldine, R.S., Giles, M.R., Brown, S. (Eds.), Geology of the Brent Group. The Geological Society, London, pp. 289-327.

Hiller, K., Elahi, M., 1984. Structural development and hydrocarbon entrapment in the Surma Basin, Bangladesh (north-east Indo-Burman fold belt), Proceedings of the 5th Offshore South Asia Conference, Singapore.

Hirt, W.G., Wenk, H.R., Boles, J.R., 1993. Albitization of plagioclase crystals in the Stevens Sandstone (Miocene), San Joaquin Basin, California and the Frio Formation (Oligocene), Gulf Coast, Texas, a TEM AEM study. Geological Society of America Bulletin 105, 708-714.

Houseknecht, D.W., 1987. Assessing the relative importance of compaction processes and cementation to reduction of porosity in sandstones. American Association of Petroleum Geologists Bulletin 71, 633-642.

Imam, M.B., Shaw, H.F., 1987. Diagenetic controls on the reservoir propoerties of gas bearing Neogene Surma Group sandstones in the Bengal Basin, Bangladesh. Marine and Petroleum Geology 4, 103-111.

Irwin, H., Curtis, C., Coleman, M.L., 1977. Isotopic evidence for source of diagenetic carbonates formed during burial of organic rich sediments. Nature 269, 209-213.

Islam, M.A., 2009. Diagenesis and reservoir quality of Bhuban sandstones (Neogene), Titas Gas Field, Bengal Basin, Bangladesh. Journal of Asian Earth Sciences 35, 89-100.

Islam, M.A., 2010. Petrophysical Evaluation of Subsurface Reservoir Sandstones of Bengal Basin, Bangladesh. Journal of the Geological Society of India 76, 621-631.

Johnson, S.Y., Alam, A.M.N., 1991. Sedimentation and tectonics of the Sylhet Trough, Bangladesh. Geological Society of America Bulletin 103, 1513-1527.

Jokat, W., Nogi, Y., Leinweber, V., 2010. New aeromagnetic data from the western Enderby Basin and consequences for Antarctic-India break-up. Geophysical Research Letters 37.

Keller, W.D., Reynolds, R.C., Inoue, A., 1986. Morphology of clay minerals in the smectite-to-illite conversion series by scanning electron microscope. Clays and Clay Minerals 34, 187-197.

Khan, M.A.M., Ismail, M., Ahmed, M., 1988. Geology and hydrocarbon prospects of the Surma Basin, Bangladesh, 7th Offshore South Asia Conference, Singapore, pp. 364-387.

Lemon, N.M., Cubitt, C.J., 2003. Illite fluorescence microscopy: a new technique in the study of illite in the Merrimelia Formation. Cooper Basin, Australia, in: Worden, R.H., Morad, S. (Eds.), Clay mineral cements in sandstones. International Association of Sedimentolgists Special Publication. Blackwells, Oxford, pp. 411-424.

Lietz, J.K., Kabir, J., 1982. Prospects and constraints of oil exploration in Bangladesh, 4th Offshore South East Asia Conference, Singapore, pp. 1-4.

Matlack, K.S., Houseknecht, D.W., Applin, K.R., 1989. Emplacement of clay into sand by infiltration. Journal of Sedimentary Petrology 59, 77-87.

McBride, E.F., 1989. Quartz cement in sandstones: a review. Earth Science Reviews 26, 69-112.

McIlroy, D., Worden, R.H., Needham, S.J., 2003. Faeces, clay minerals and reservoir potential. Journal of the Geological Society 160, 489-493.

McKinley, J.M., Worden, R.H., Ruffell, A.H., 2003. Smectite in sandstones: A review of the controls on occurrence and behaviour during diagenesis. In: Clay mineral cements in sandstones (eds. Worden, R.H. and Morad, S.) International Association of Sedimentologists Special Publications 34, 109-128.

Morad, S., 1998. Carbonate cementation in sandstones: distribution patterns and geochemical evolution. In: Carbonate cementation in sandstones (ed. Morad, S.) International Association of Sedimentologists Special Publications 26, 1-26.

Morad, S., De Ros, L.F., 1994. Geochemistry and diagenesis of stratabound calcite cement layers within the Rannoch Formation of the Brent Group, Murchison Field, North Viking Graben (Northern North Sea) - Comment. Sedimentary Geology 93, 135-141.

Morad, S., Ketzer, J.M., De Ros, L.F., 2000. Spatial and temporal distribution of diagenetic alterations in siliciclastic rocks: implications for mass transfer in sedimentary basins. Sedimentology 47, 95-120.

Moraes, M.A.S., De Ros, L.F., 1990. Infiltrated clays in fluvial Jurassic sandstones of Recôncavo Basin, northeastern Brazil. Journal of Sedimentary Petrology 60, 809-819.

Moraes, M.A.S., De Ros, L.F., 1992. Depositional, infiltrated and authigenic clays in fluvial sandstones of the Jurassic Sergie Formation, Reconcavo Basin, northeastrn Brazil, In: Origin, diagenesis and petrophysics of clay minerals in sandstones (eds. Houseknecht, D.W. and Pittman, E.D.) SEPM Special Publication, pp. 197-208.

Needham, S.J., Worden, R.H., McIlroy, D., 2005. Experimental production of clay rims by macrobiotic sediment ingestion and excretion processes. Journal of Sedimentary Research 75, 1028-1037.

Osborne, M.J., Swarbrick, R.E., 1999. Diagenesis in North Sea HPHT elastic reservoirs - consequences for porosity and overpressure prediction. Marine and Petroleum Geology 16, 337-353.

Paxton, S.T., Szabo, J.O., Ajdukiewicz, J.M., Klimentidis, R.E., 2002. Construction of an intergranular volume compaction curve for evaluating and predicting compaction and porosity loss in rigid-grain sandstone reservoirs. American Association of Petroleum Geologists Bulletin 86, 2047-2067.

Rahman, M.J.J., Faupl, P., Alam, M.M., 2009. Depositional facies of the subsurface Neogene Surma Group in the Sylhet Trough of the Bengal Basin, Bangladesh: record of tidal sedimentation. International Journal of Earth Sciences 98, 1971-1980.

Rahman, M.J.J., McCann, T., 2012. Diagenetic history of the Surma Group sandstones (Miocene) in the Surma Basin, Bangladesh. Journal of Asian Earth Sciences 45, 65-78.

Rahman, M.J.J., McCann, T., Abdullah, R., Yeasmin, R., 2011. Sandstone diagenesis of the Neogene Surma Group from the Shahbazpur gas field, Southern Bengal Basin, Bangladesh. Austrian Journal of Earth Sciences 104, 114-126.

Ramm, M., Bjorlykke, K., 1994. Porosity depth trends in Norwegain reservoirs - assessing the quantitative effects of varying pore-pressure, temperature history and mineralogy, Norwegian shelf data. Clay Minerals 29, 475-490.

Ramm, M., Forsberg, A.W., Jahren, J., 1997. Porosity-depth trends in deeply buried Upper Jurassic Reservoirs in the Norwegian Central Graben: an example of porosity preservation beneath the normal economic basement by grain coating microquartz. In: Reservoir quality prediction in sandstones and carbonates (eds. Kupecz, J.A., Gluyas, J. and Bloch, S.) AAPG Memoir 69, 177-200.

Shamsuddin, A.H.M., Brown, T., Lee, S., Curiale, J., 2001. Petroleum Systems of Bangladesh, Proceedings of the 13th Southeast Asia petroleum Exploration Society (SEAPEX) Exploration Conference, Singapore.

Tucker, M.E., 1988. Techniques in Sedimentology, in: Tucker, M.E. (Ed.). Blackwell Science Ltd.

Uddin, A., Lundberg, N., 1998. Cenozoic history of the Himalayan-Bengal system: Sand composition in the Bengal basin, Bangladesh. Geological Society of America Bulletin 110, 497-511.

Walderhaug, O., Lander, R.H., Bjorkum, P.A., Oelkers, E.H., Bjorlykke, K., Nadeau, P.H., 2000. Modelling quartz cementation and porosity in reservoir sandstones: examples from the Norwegain continental shelf. In: Quartz cementation in sandstones (eds. Worden, R.H. and Morad, S.) International Association of Sedimentologists Special Publications 29, 39-50.

Worden, R.H., Barclay, S.A., 2000. Internally-sourced quartz cement due to externally-derived CO2 in sub-arkosic sandstones, North Sea. Journal of Geochemical Exploration 69, 645-649.

Worden, R.H., Burley, S.D., 2003. Sandstone diagenesis: the evolution from sand to stone, in: Burley, S.D., Worden, R.H. (Eds.), Sandstone diagenesis, recent and ancient. International Association of Sedimentologists Reprint Series, pp. 3-44.
Worden, R.H., Mayall, M., Evans, I.J., 2000. The effect of ductile-lithic sand grains and quartz cement on porosity and permeability in Oligocene and lower Miocene clastics, South China Sea: Prediction of reservoir quality. American Association of Petroleum Geologists Bulletin 84, 345-359.
Worden, R.H., Mayall, M.J., Evans, I.J., 1997. Predicting reservoir quality during exploration: lithic grains, porosity and permeability in Tertiary clastics of the South China Sea basin, in: A.J., F., Matthews, A.J., Murphy, R.W. (Eds.), Petroleum Geology of S E Asia. Special Publication. Geological Society, London, pp. 107-115.
Worden, R.H., Morad, S., 2000. Quartz cementation in sandstones: a review of the key controversies In: Quartz cementation in sandstones (eds. Worden, R.H. and Morad, S.) International Association of Sedimentologists Special Publications, pp. 1-20.
Worden, R.H., Morad, S., 2003. Clay minerals in sandstones: Controls on formation, distribution and evolution. In: Clay mineral cements in sandstones (eds. Worden, R.H. and Morad, S.) International Association of Sedimentologists Special Publications 34, 3-41.
Worden, R.H., Needham, S.J., Cuadros, J., 2006. The worm gut; a natural clay mineral factory and a possible cause of diagenetic grain coats in sandstones. Journal of Geochemical Exploration 89, 428-431.
Worden, R.H., Oxtoby, N.H., Smalley, P.C., 1998. Can oil emplacement prevent quartz cementation in sandstones? Petroleum Geoscience 4, 129-137.
Worden, R.H., Warren, E.A., Smalley, P.C., Primmer, T.J., Oxtoby, N.H., 1995. Evidence for resetting of fluid inclusions from quartz cements in oil fields - discussion. Marine and Petroleum Geology 12, 566-570.

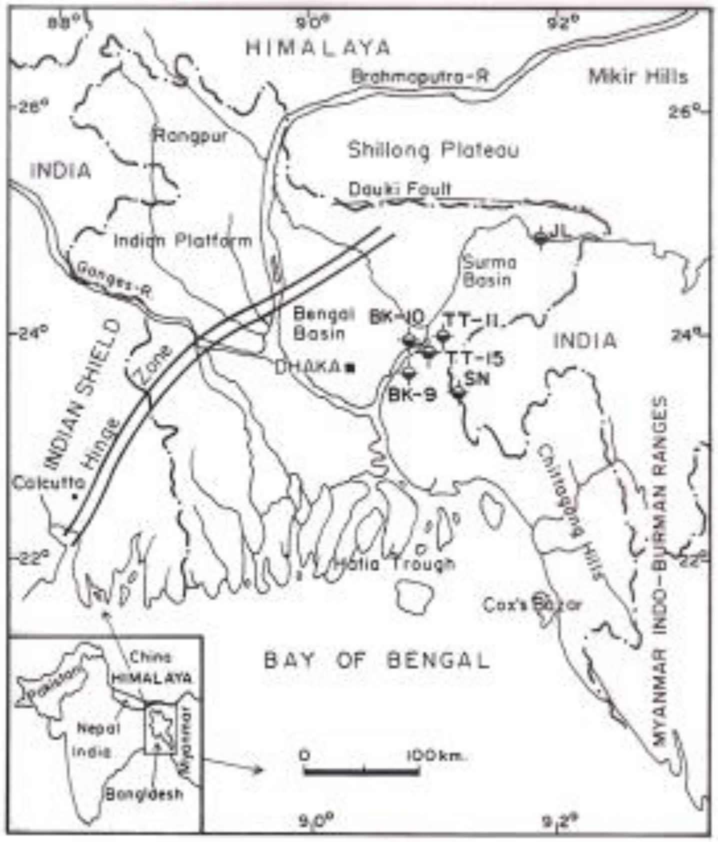
HIMALAYA
Brahmaputra-R
Mikir Hills
Shillong Plateau
Dauki Fault
INDIA
Rangpur
Indian Platform
Ganges-R
Surma
Basin
Bengal
Basin
BK-10
TT-11
TT-15
BK-9
SN
JL
DHAKA
INDIA
INDIAN SHIELD
Hinge
Zone
Calcutta
Hatia Trough
Chittagong Hills
MYANMAR INDO-BURMAN RANGES
Cox's Bazar
BAY OF BENGAL
0
100km.
China
HIMALAYA
Pakistan
Nepal
India
Myanmar
Bangladesh
88°
90°
92°
26°
24°
22°

Figure 1

874

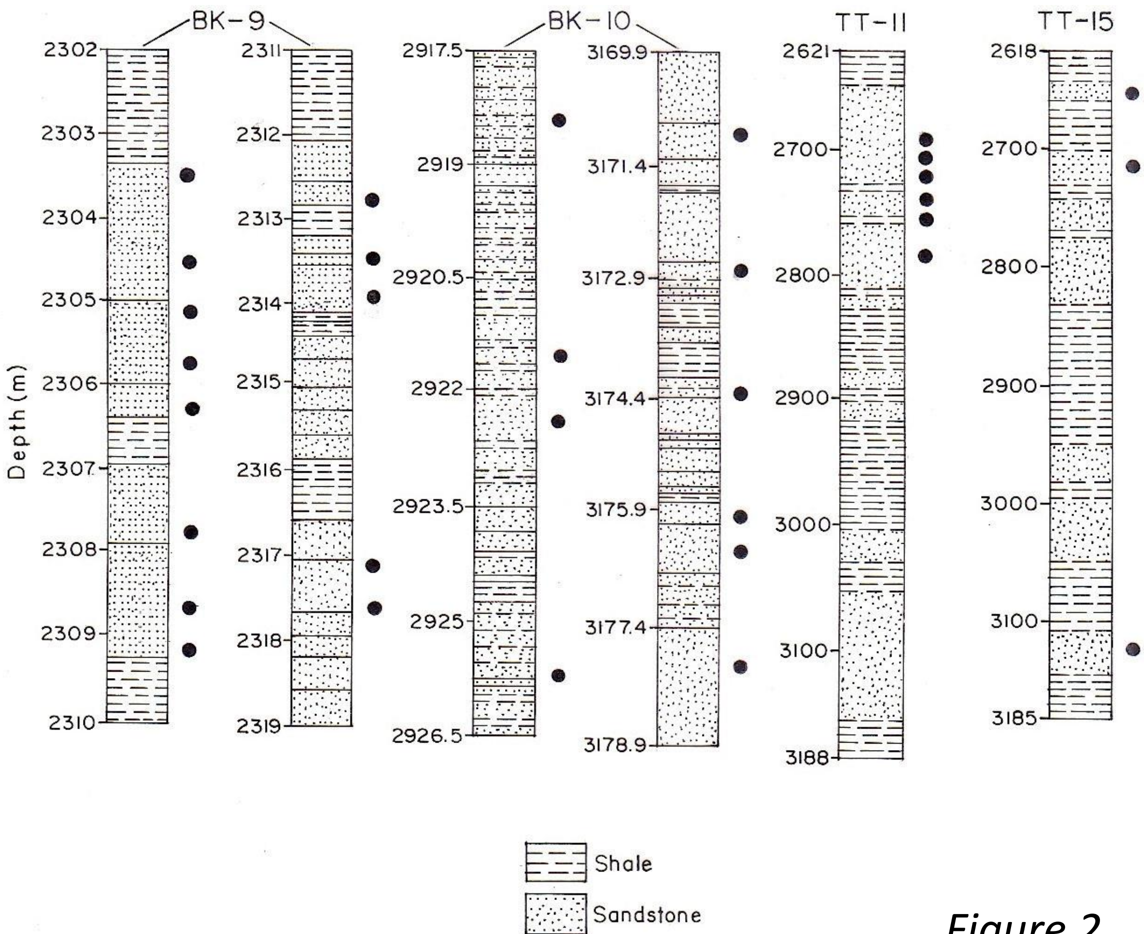
BK-9
BK-10
TT-11
TT-15
Depth (m)
2302
2303
2304
2305
2306
2307
2308
2309
2310
2311
2312
2313
2314
2315
2316
2317
2318
2319
2917.5
2919
2920.5
2922
2923.5
2925
2926.5
3169.9
3171.4
3172.9
3174.4
3175.9
3177.4
3178.9
2621
2700
2800
2900
3000
3100
3188
2618
2700
2800
2900
3000
3100
3185
Shale
Sandstone

Figure 2

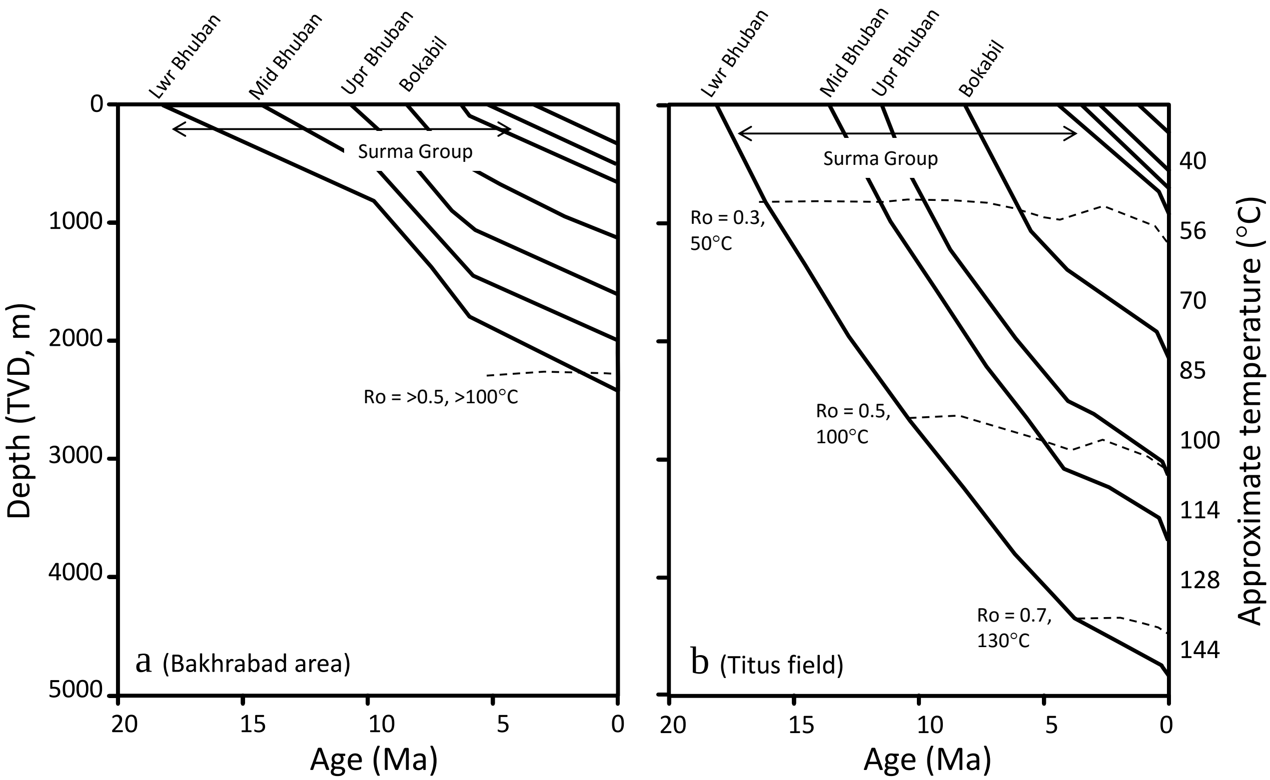
Lwr Bhuban
Mid Bhuban
Upr Bhuban
Bokabil
Surma Group
Ro = >0.5, >100°C
a (Bakhrabad area)
Depth (TVD, m)
Age (Ma)
Ro = 0.3,
50°C
Ro = 0.5,
100°C
Ro = 0.7,
130°C
b (Titus field)
Approximate temperature (°C)

Figure 3

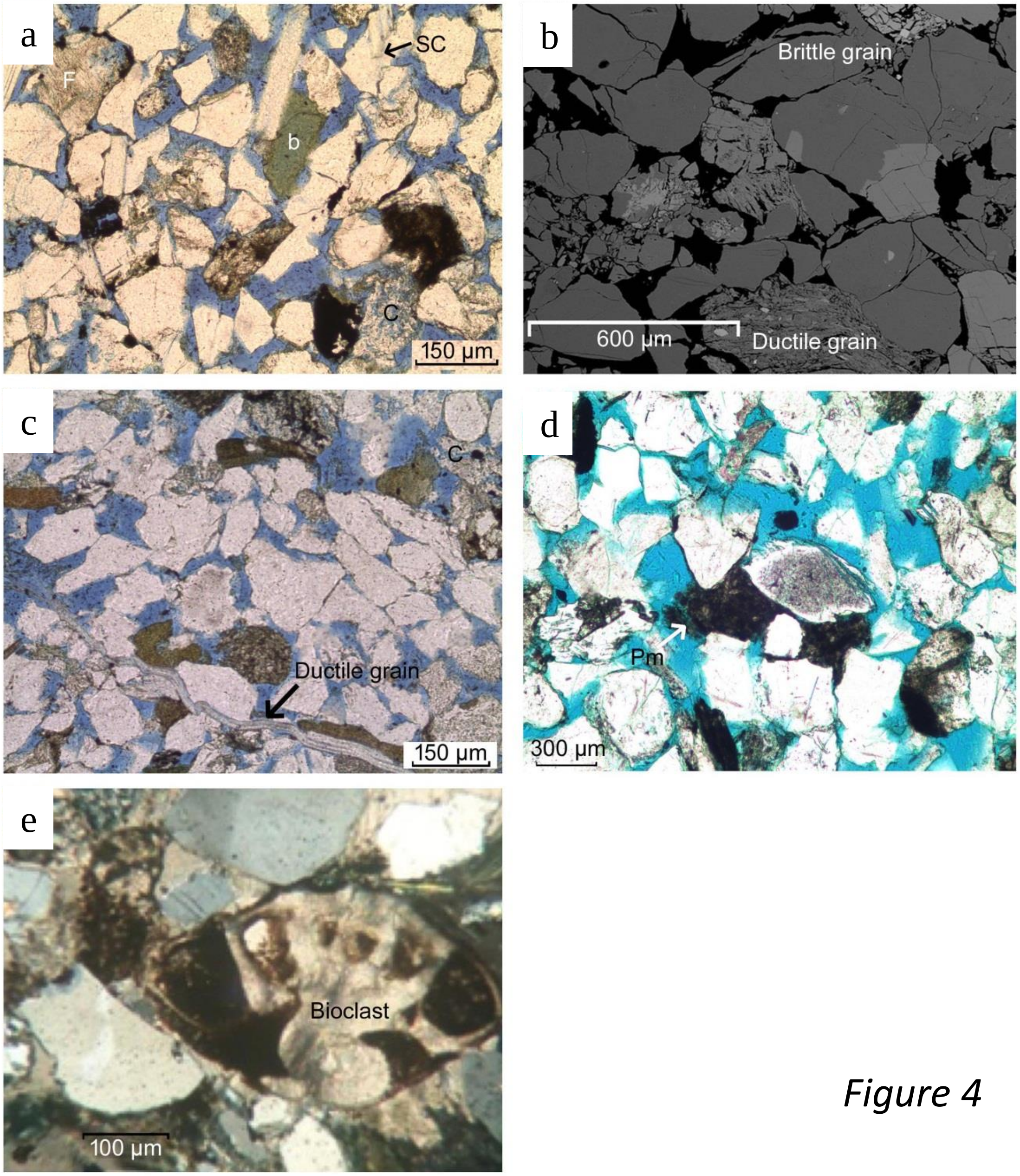
a
SC
F
b
C
150 µm
b
Brittle grain
600 µm
Ductile grain
c
C
Ductile grain
150 µm
d
Pm
300 µm
e
Bioclast
100 µm

Figure 4

Figure 5

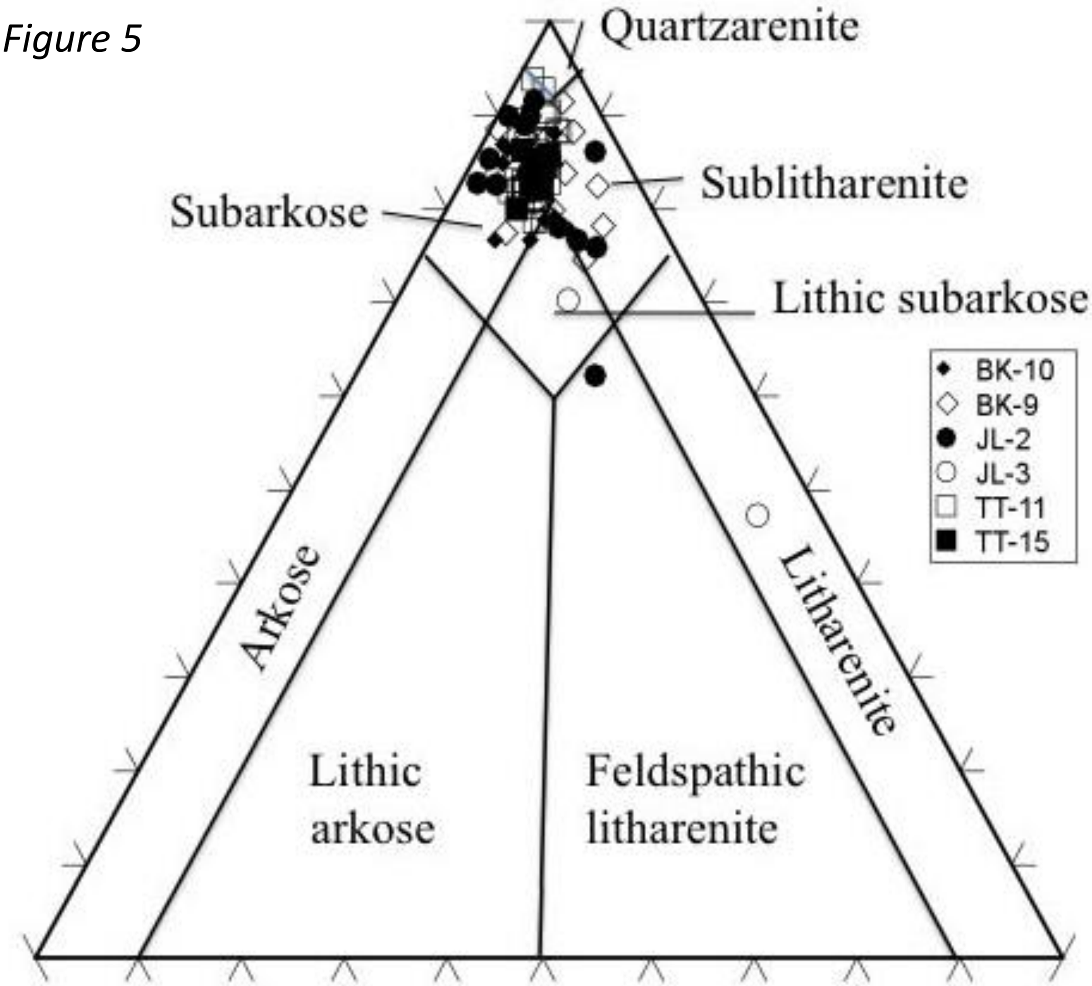
Quartzarenite
Sublitharenite
Subarkose
Lithic subarkose
BK-10
BK-9
JL-2
JL-3
TT-11
TT-15
Arkose
Litharenite
Lithic arkose
Feldspathic litharenite

878

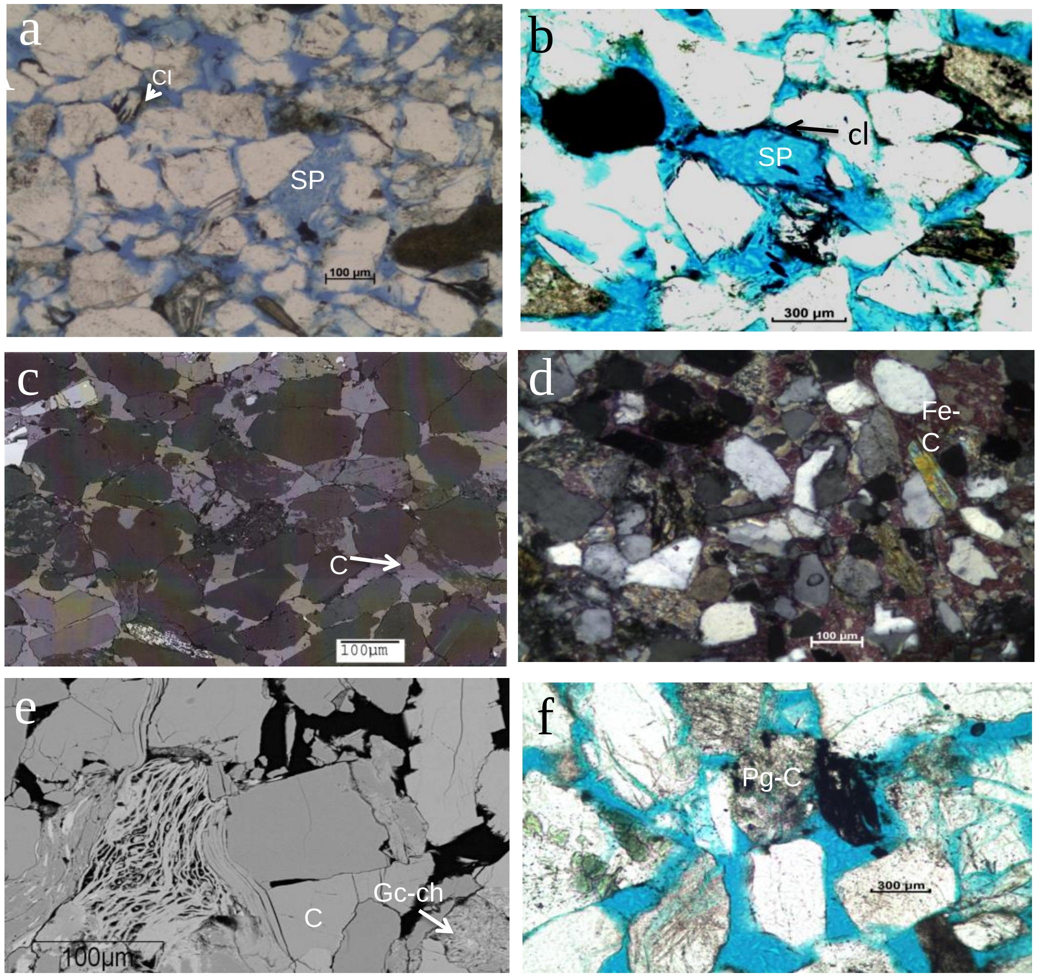

a
Cl
SP
100 µm
b
cl
SP
300 µm
c
C
100µm
d
Fe-
C
100 µm
e
C
Gc-ch
100µm
f
Pg-C
300 µm

Figure 6

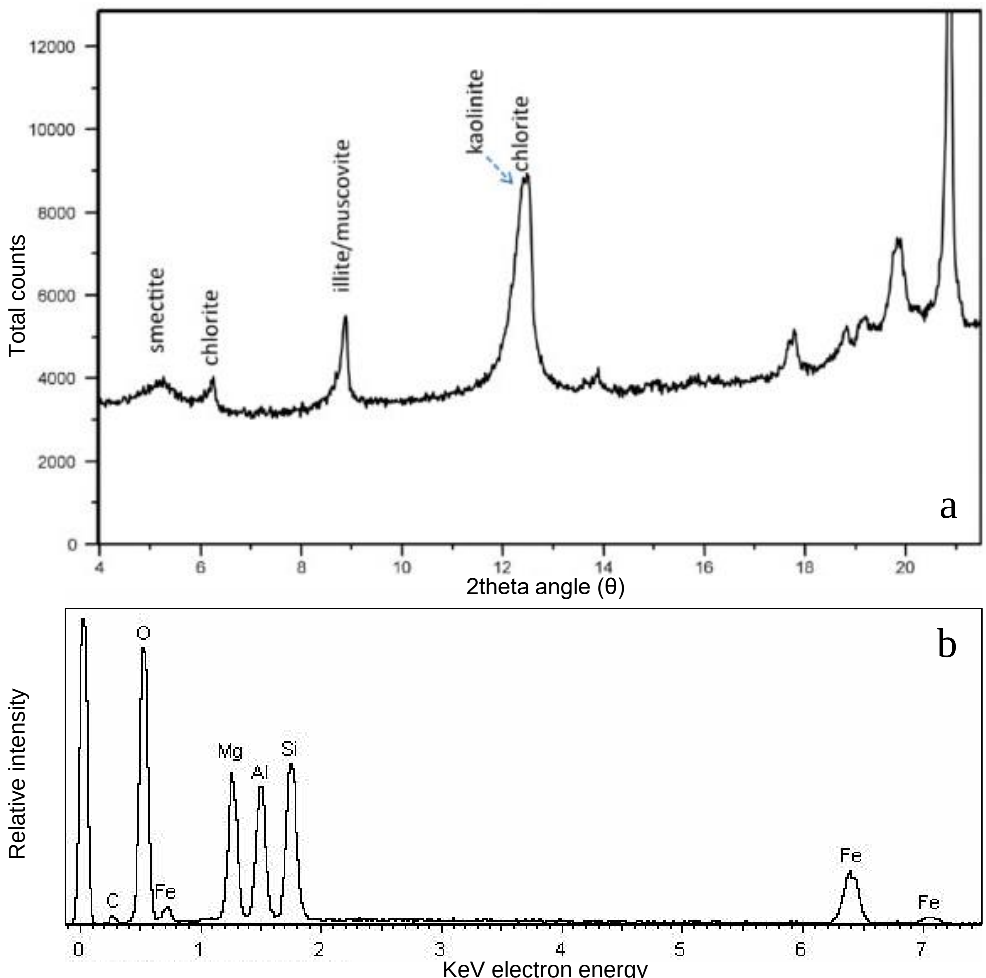
Total counts
12000
10000
8000
6000
4000
2000
0
smectite
chlorite
illite/muscovite
kaolinite
chlorite
a
4
6
8
10
12
14
16
18
20
2theta angle (θ)
b
Relative intensity
O
C
Fe
Mg
Al
Si
Fe
Fe
0
1
2
3
4
5
6
7
KeV electron energy

Figure 7

879

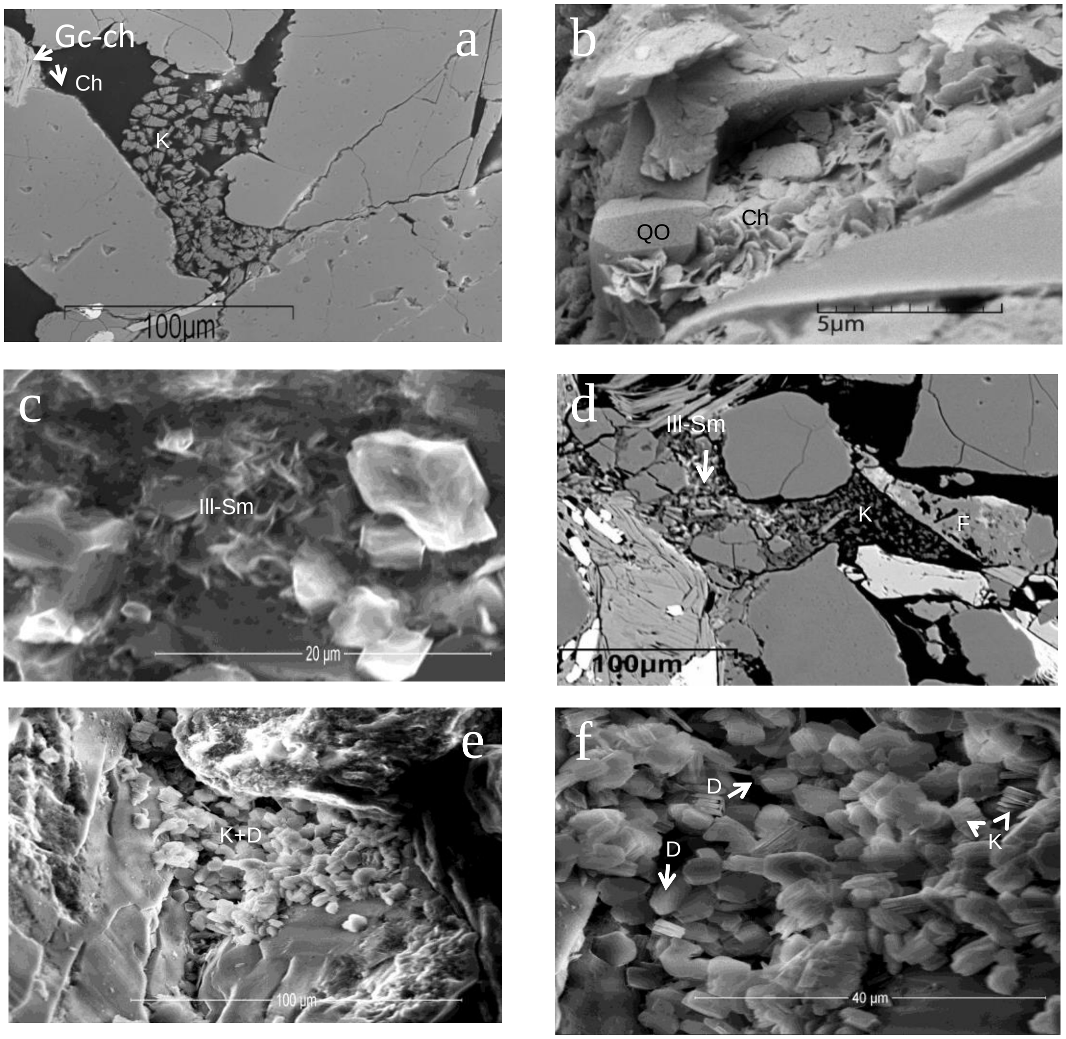
a
Gc-ch
Ch
K
100µm
b
QO
Ch
5µm
c
Ill-Sm
20 µm
d
Ill-Sm
K
F
100µm
e
K+D
100 µm
f
D
D
K
40 µm

Figure 8

881

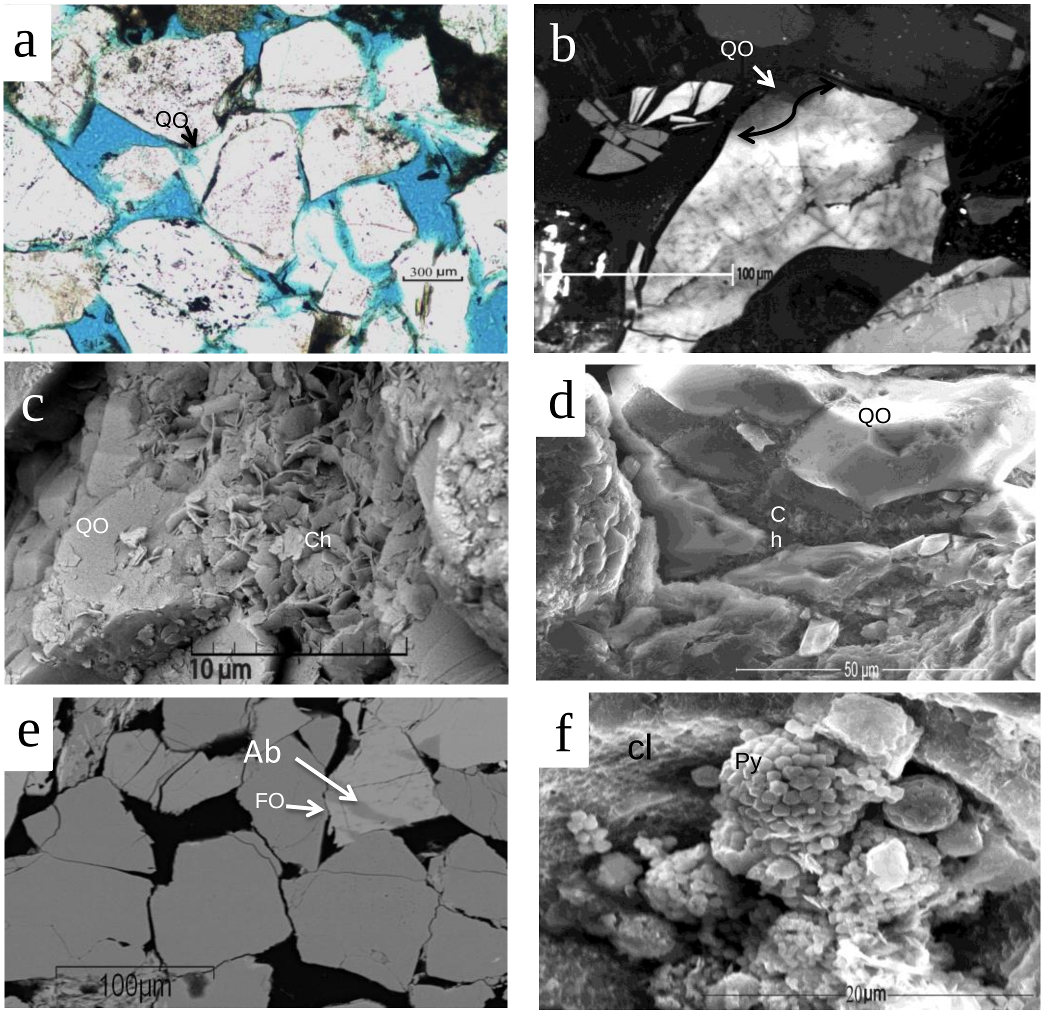
a
QO
300 µm
b
QO
100 µm
c
QO
Ch
10 µm
d
QO
C
h
50 µm
e
Ab
FO
100µm
f
cl
Py
20µm

Figure 9

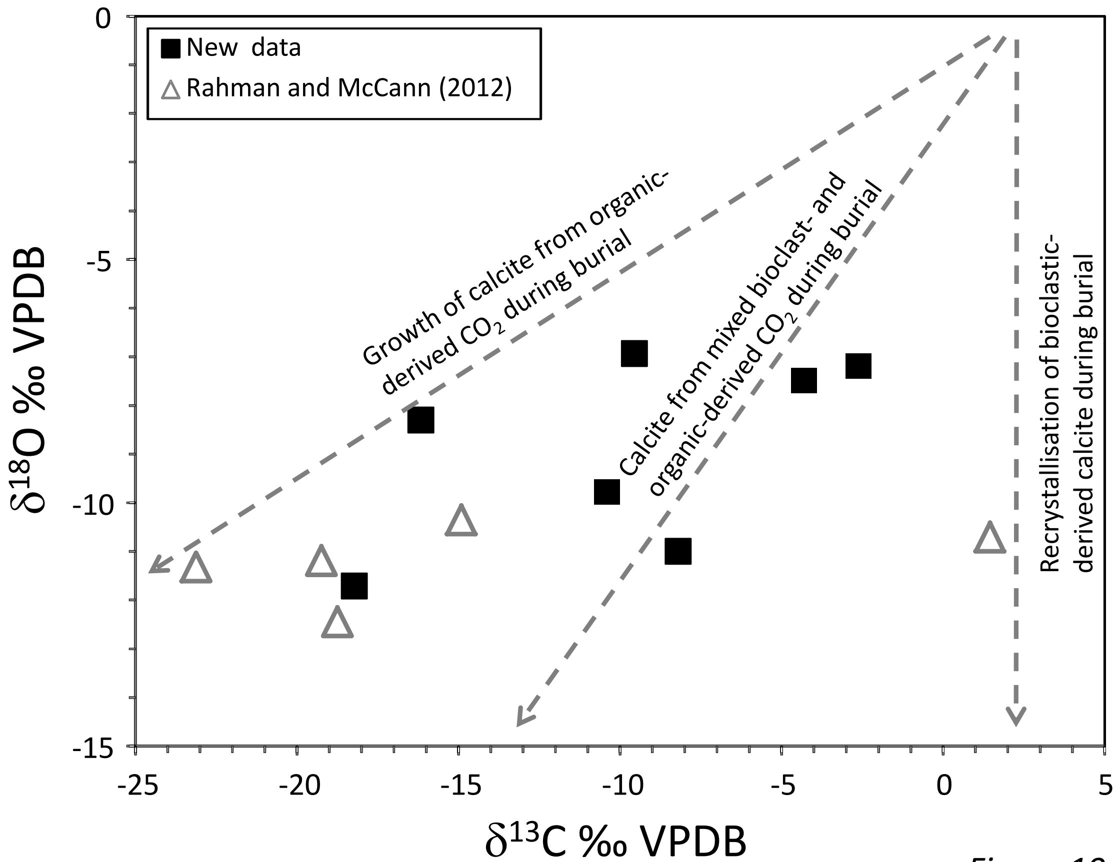
New data
Rahman and McCann (2012)
Growth of calcite from organic-derived CO_2 during burial
Calcite from mixed bioclast- and organic-derived CO_2 during burial
Recrystallisation of bioclastic-derived calcite during burial
$\delta^{18}O$ ‰ VPDB
$\delta^{13}C$ ‰ VPDB
0
-5
-10
-15
-25
-20
-15
-10
-5
0
5

Figure 10

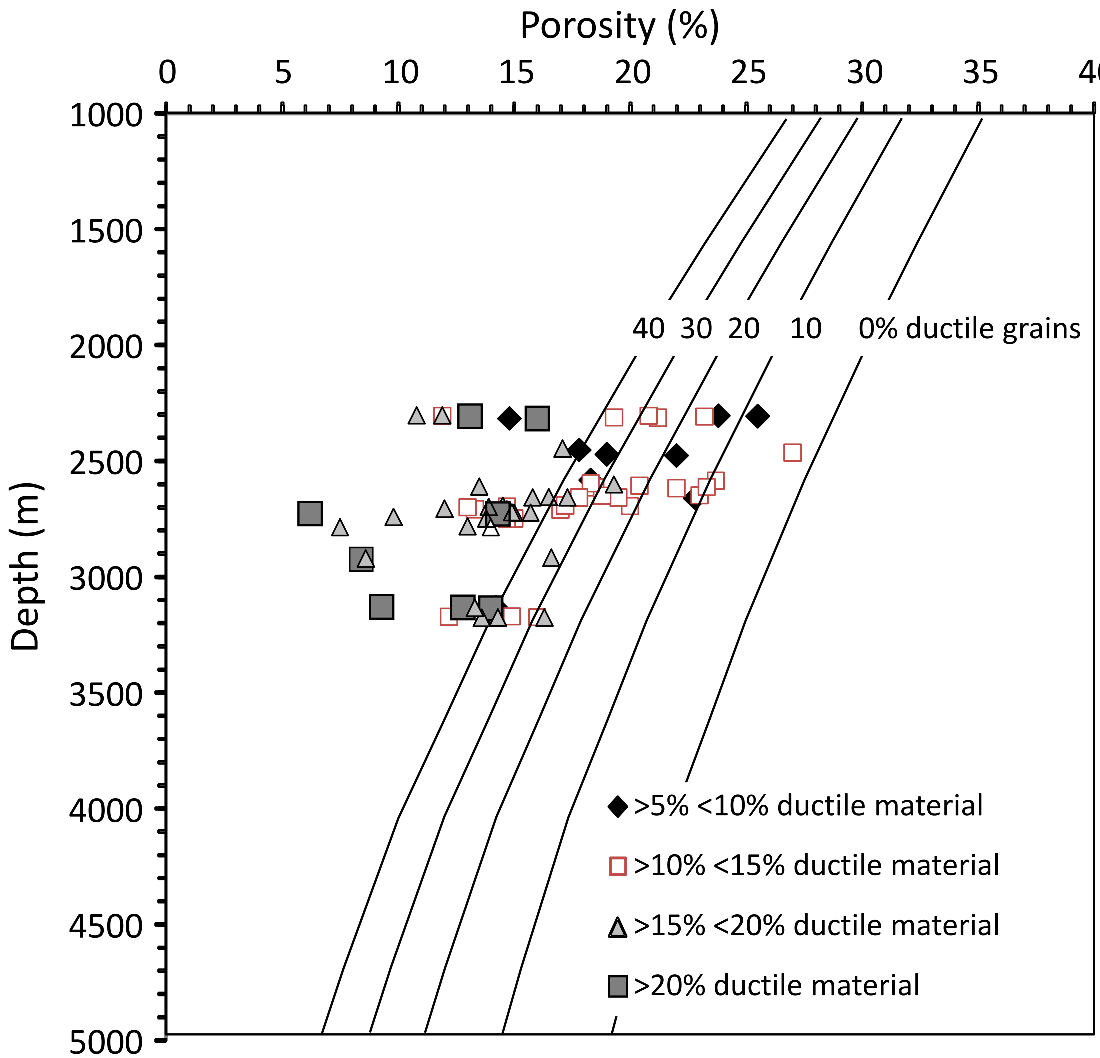

Figure 11

884

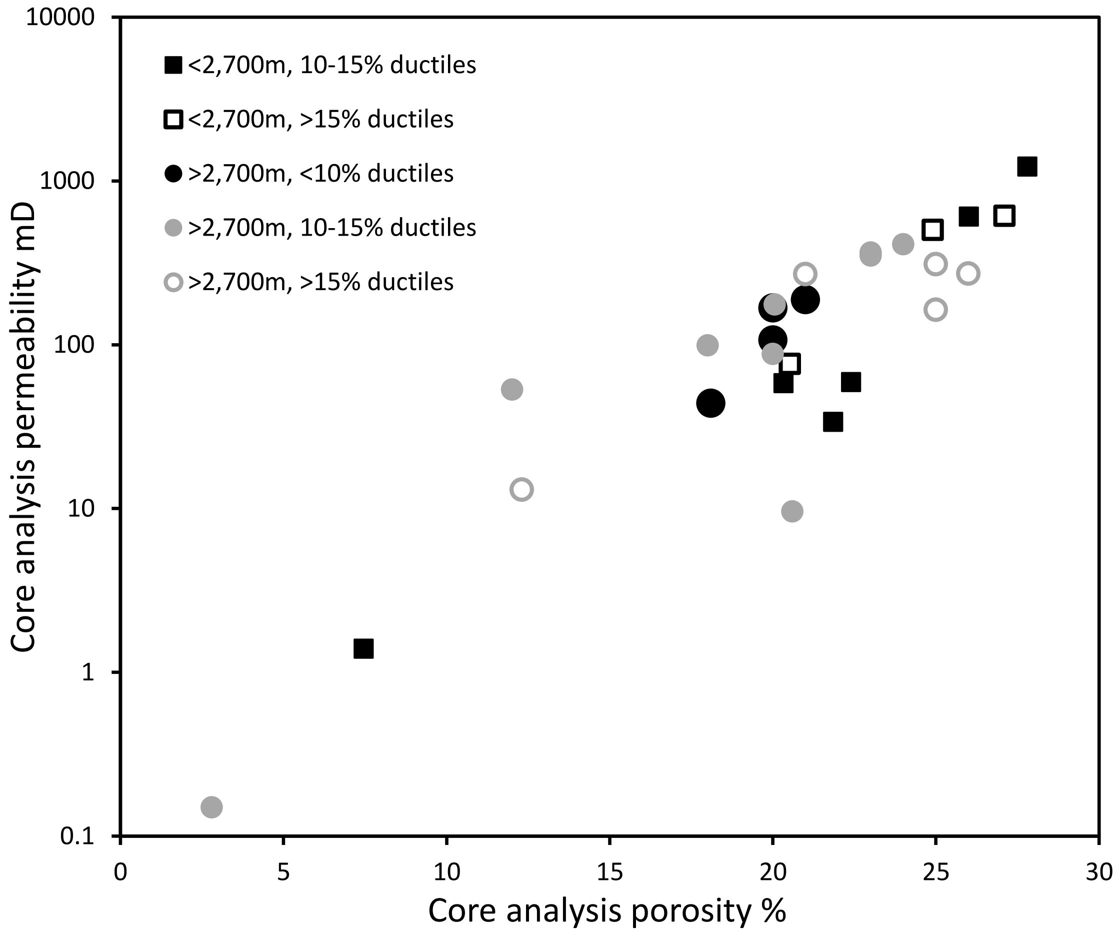

Figure 12

885

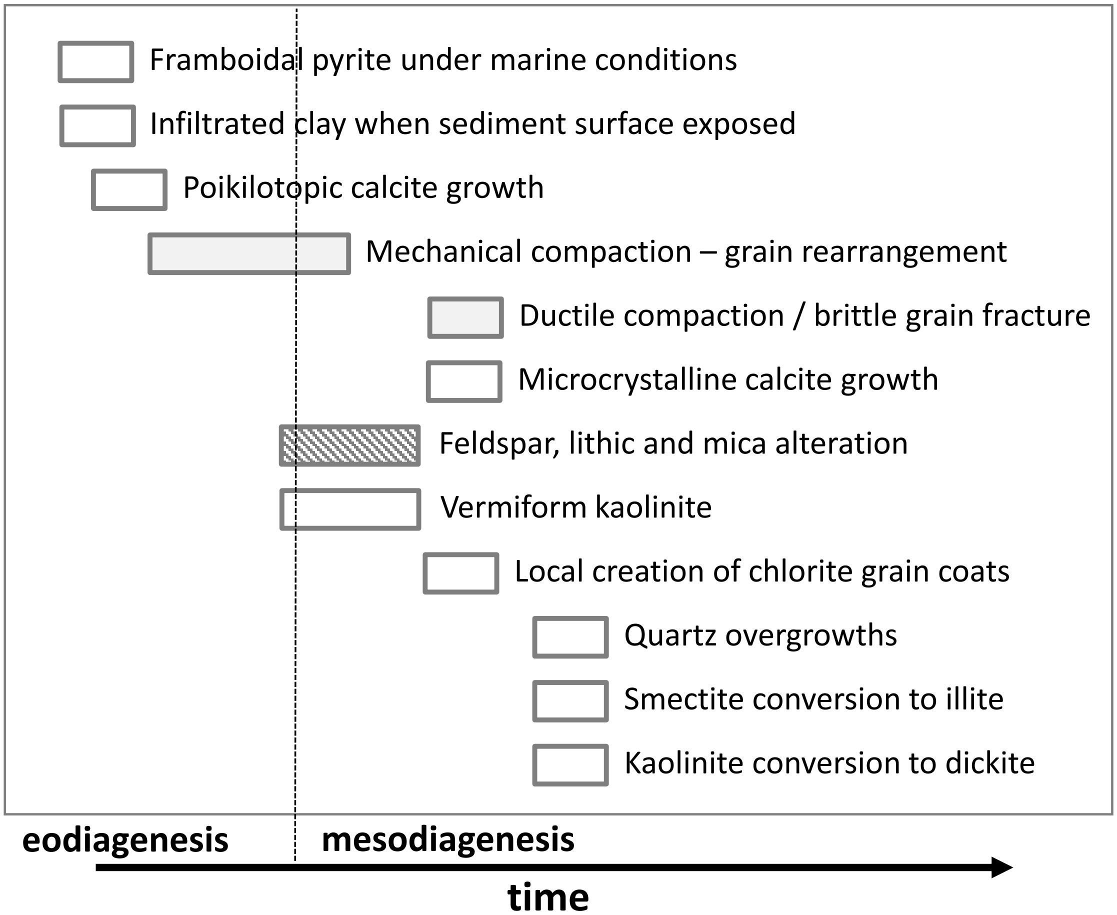

Figure 13

886

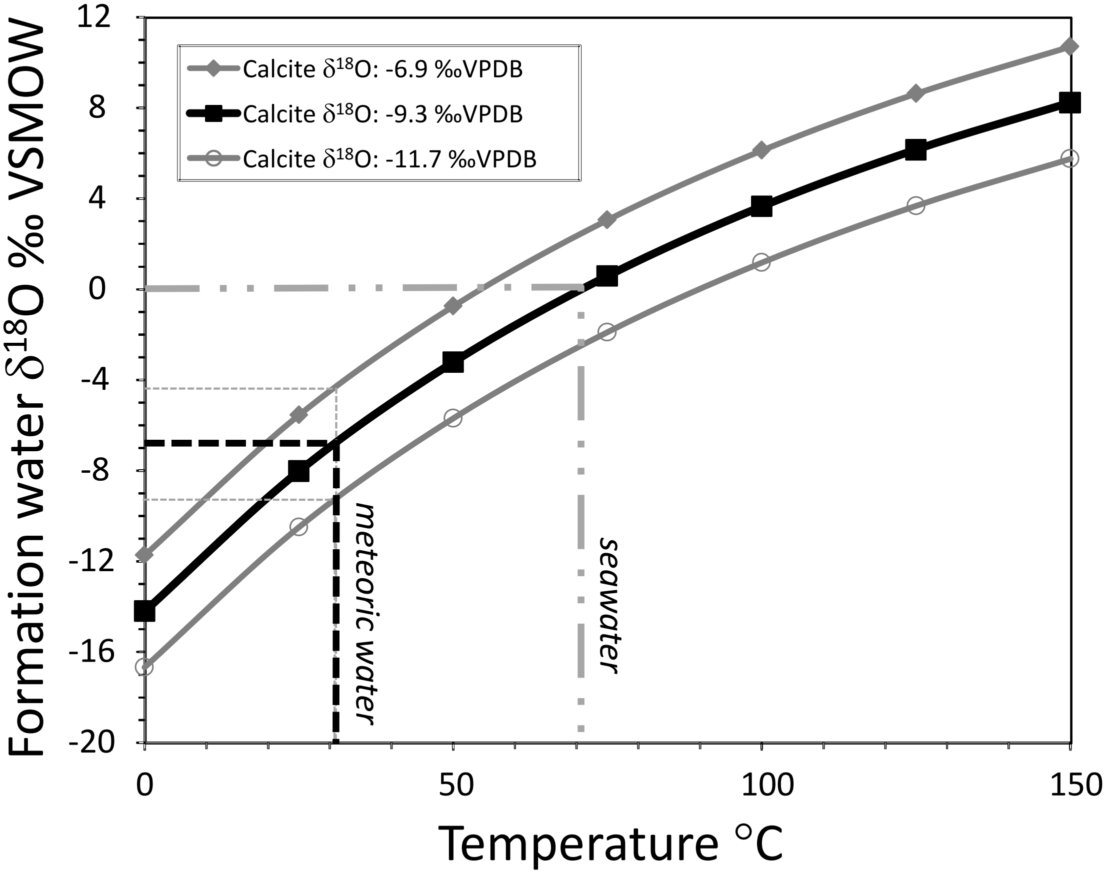

Figure 14

887

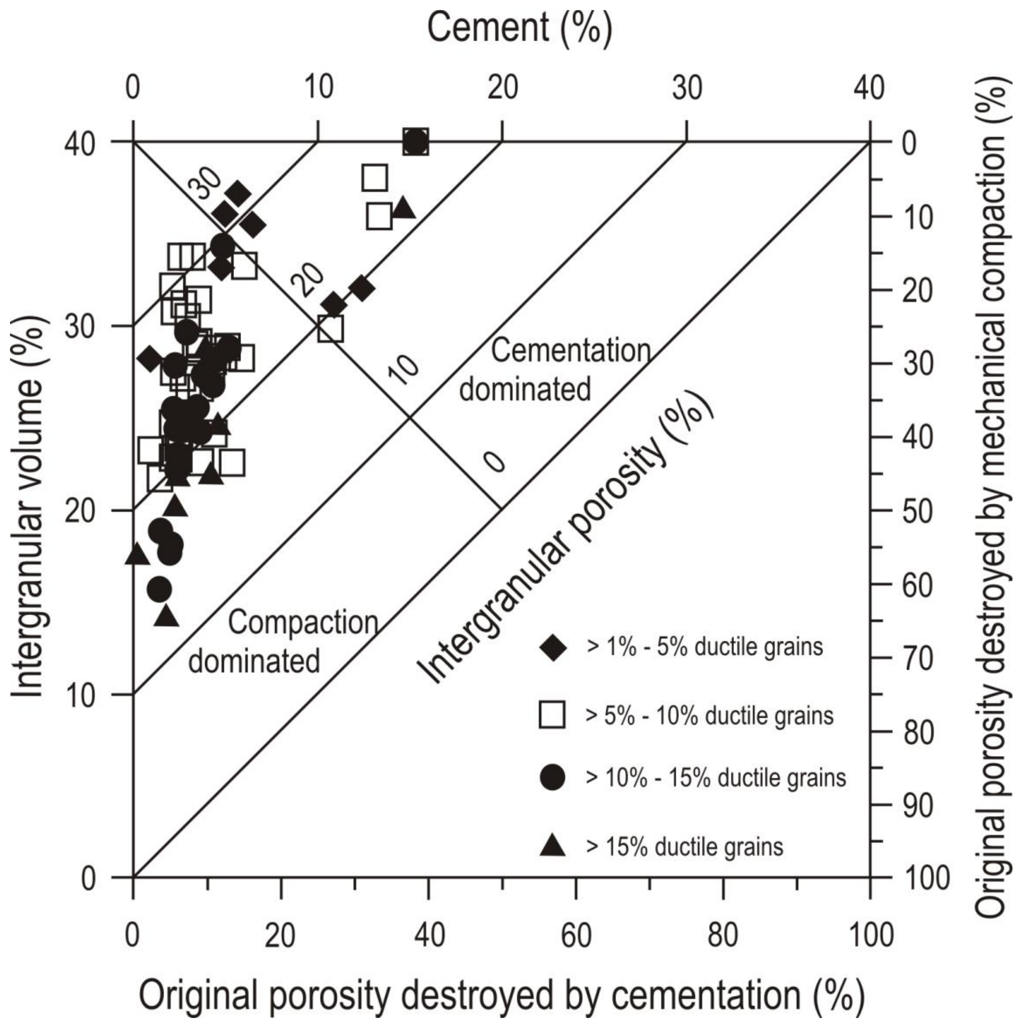

Figure 15

888

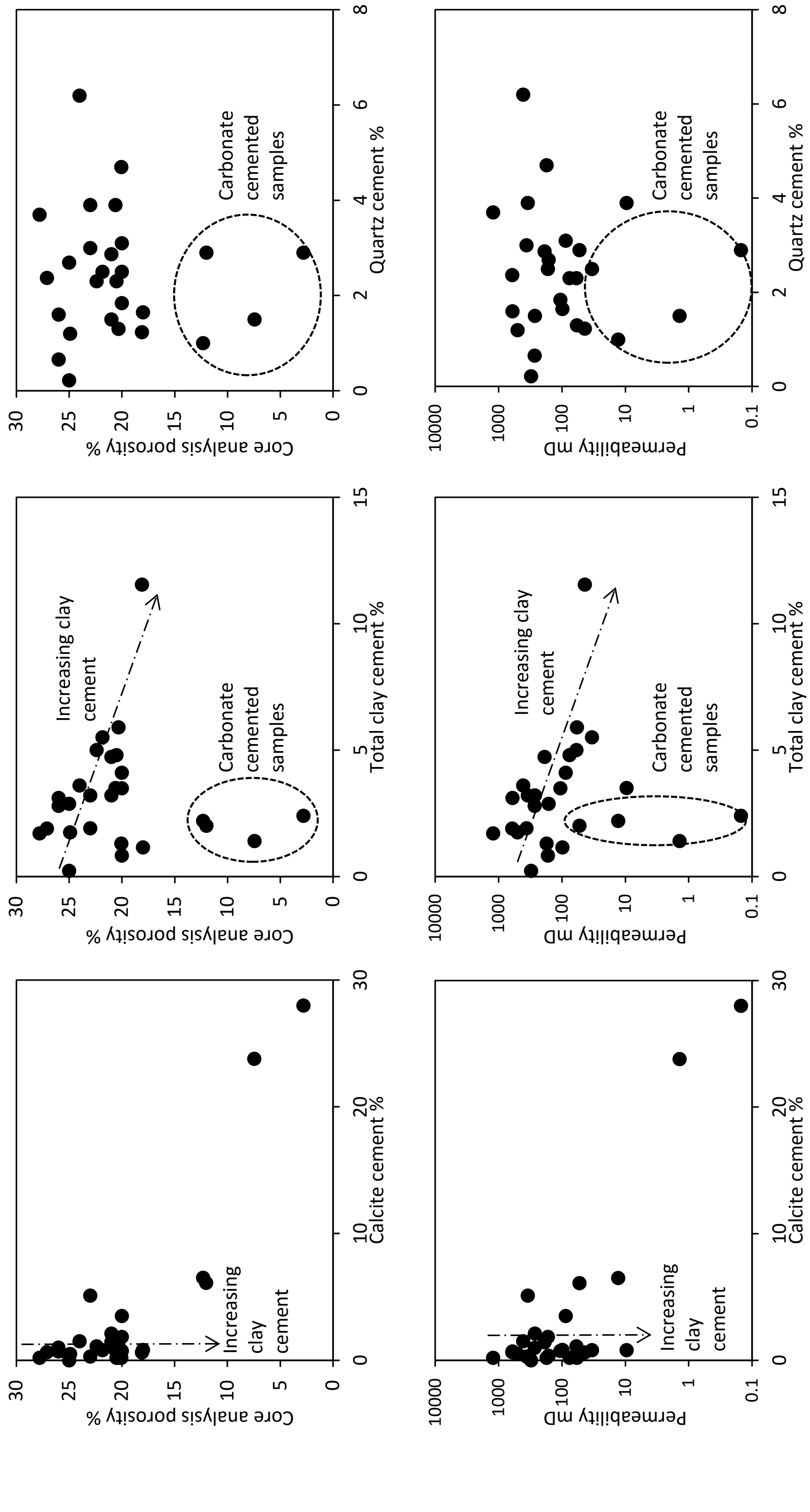

Core analysis porosity %
Permeability mD
Calcite cement %
Total clay cement %
Quartz cement %
Increasing clay cement
Carbonate cemented samples

Figure 16

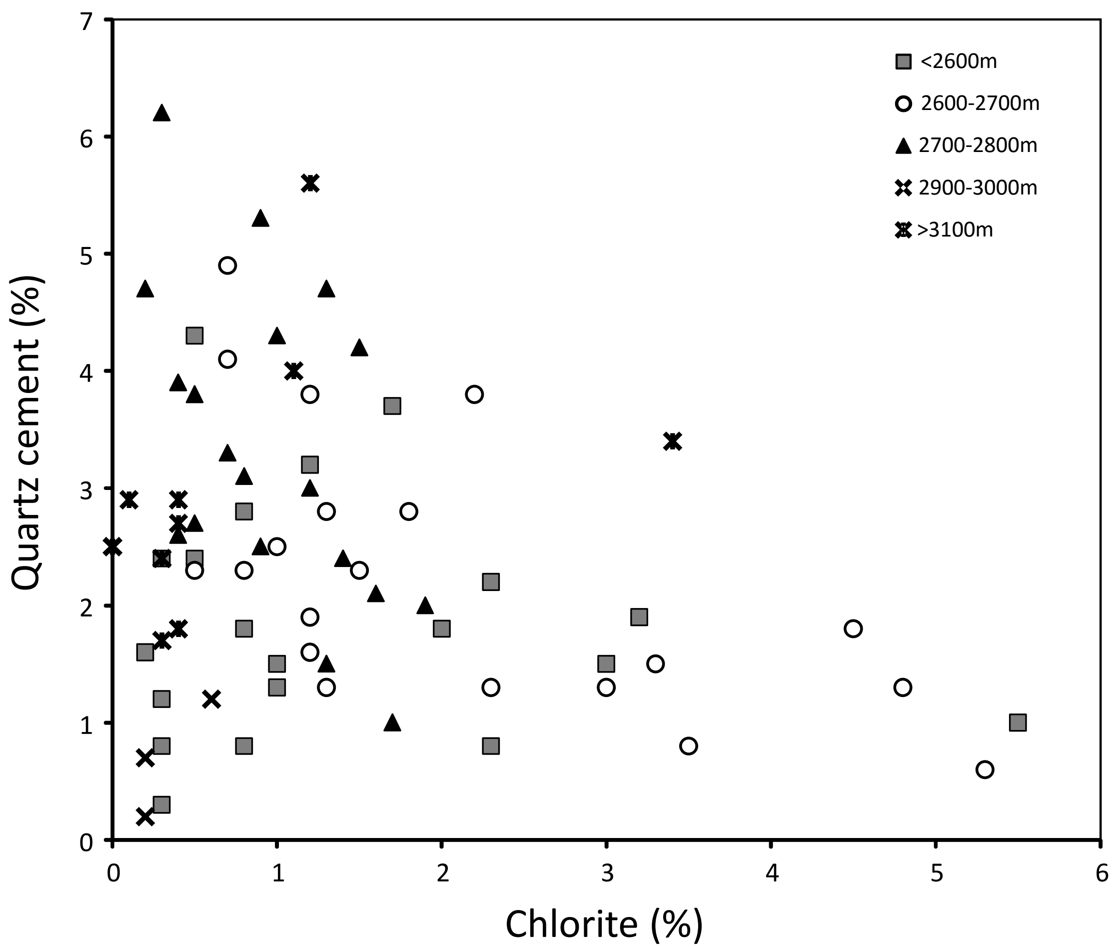

<2600m
2600-2700m
2700-2800m
2900-3000m
>3100m
Quartz cement (%)
Chlorite (%)
0
1
2
3
4
5
6
7

Figure 17

Table 1 Stratigraphic succession of the Bengal Basin (after Rahman and McCann, 2012).

Age (approx.)	Group/ Formation (Fm.)	Lithology	Environment o deposition
Plio-Pleistocene	Dihing Fm. Dupi Tila Fm.	Silty sandstone and claystone; boulder and pebble beds Massive sandstone and clay	Fluvial
Pliocene	Tipam Group	Massive to cross bedded sandstone, minor shale and clay	Fluvial
Miocene	Surma Group Boka Bil Fm. Bhuban Fm.	 Alternating siltstone and shale with sandstone Alternation of siltstone with shale and sandstone Silty and sandy shale Sandstone and sandy shale Unconformity	Deltaic-shallow marine
Oligocene	Barail Group	Sandstone, shale, coal	Deltaic-shallow marine
Paleocene-Eocene	Jaintia Group	Limestone, sandstone, shale	Open marine

Table 2 (part 1)

Well	Depth (m)	Quartz monocrystalline	Quartz polycrystalline	Chert	K-feldspar	Plagioclase	Detrital Biotite	Detrital muscovite	Lithics-sedimentary	Lithics metamorphic	Lithics volcanic	Detrital carbonate clasts	Matrix clay	Quartz cement	Chlorite cement	Calcite cement	Clay cements	Primary porosity	Secondary porosity	IGV	$\delta^{13}C$ ‰ VPDB	$\delta^{18}O$ ‰ VPDB	core analysis porosity %	core analysis permeability mD
JL-2(1)	2582.0	38.7	14.3	1.5	1.8	6.8	0.0	0.5	0.7	0.0	0.2	0.5	3.0	0.8	2.3	4.5	4.3	18.3	2.3	33.2				
JL-2(2)	2588.0	36.5	6.9	1.1	2.2	3.6	0.3	0.0	5.0	1.7	0.0	3.6	2.0	2.8	0.8	2.2	2.2	23.7	4.5	33.7				
JL-2(4)	2595.3	28.9	6.0	2.8	4.9	3.9	1.8	0.4	3.5	10.6	0.0	0.0	0.0	0.0	5.7	26.5	4.3	0.0	0.0	36.5	-18.2	-11.7		
JL-2(6)	2597.0	36.5	6.3	0.0	3.0	2.3	2.0	0.0	2.5	0.5	0.0	0.5	1.5	1.0	5.5	*11.8	6.3	18.3	2.0	32.5				
JL-2(7)	2603.0	34.3	6.5	0.0	1.8	1.8	1.5	1.0	2.0	1.5	0.0	0.3	1.3	1.8	4.5	*10.5	8.8	19.3	3.0	35.5				
JL-2(8)	2606.0	40.3	0.7	1.0	1.3	0.0	1.3	2.3	4.2	1.3	0.0	0.0	1.3	0.7	3.2	*19	2.6	17.0	3.6	24.8				
JL-2(9)	2608.0	36.0	7.1	1.1	2.2	3.0	1.9	0.6	5.8	2.5	0.0	1.9	1.9	3.8	2.2	4.9	1.1	20.4	2.2	34.4				
JL-2(11)	2612.0	45.5	3.8	0.9	3.3	1.7	1.4	0.9	5.4	5.5	0.0	2.5	1.8	0.6	5.3	1.2	1.9	13.5	3.2	24.3				
JL-2(12)	2613.0	35.8	3.3	0.5	3.8	3.8	1.0	1.0	0.5	0.3	0.0	1.0	4.8	0.8	3.5	8.3	6.0	23.3	2.3	46.5				
JL-2(13)	2615.0	41.5	4.8	0.5	1.5	3.8	0.5	0.5	2.3	0.0	0.0	1.0	3.3	1.3	4.8	7.3	6.0	18.5	2.5	41.0				
JL-2(14)	2619.1	40.8	4.0	0.0	2.3	1.3	0.3	0.3	0.8	0.8	0.0	1.8	1.3	2.8	1.8	9.5	7.3	22.0	3.3	44.5				
JL-2(15)	2650.0	37.3	6.0	0.0	2.0	0.8	1.3	0.5	0.3	1.0	0.0	0.3	0.8	1.3	3.0	*12.3	7.5	23.0	2.5	35.5				
JL-2(16)	2651.0	39.3	6.0	1.5	2.5	2.3	1.0	0.3	0.3	0.3	0.0	0.0	2.5	1.3	2.3	*12.3	8.3	18.8	0.8	33.1				
JL-2(17)	2659.0	35.5	7.0	0.3	3.0	4.3	1.3	1.3	0.5	1.3	0.0	0.8	2.0	1.5	3.3	*10.8	5.8	19.5	0.8	32.0				
JL-2(18)	2662.2	42.8	9.8	0.3	3.3	1.5	0.3	0.5	1.0	0.8	0.0	1.3	0.5	2.3	1.5	8.0	2.3	22.8	1.3	37.3				
JL-3(3)	2448.4	38.7	5.7	2.5	6.3	2.5	0.5	1.4	6.2	4.7	0.2	1.1	0.8	1.9	3.2	0.8	3.6	17.1	1.6	27.4				
JL-3(4)	2454.2	37.6	10.5	1.3	3.0	2.3	1.0	0.0	0.8	1.0	0.0	0.3	1.3	1.8	2.0	*13.8	3.2	17.8	2.5	26.0				
JL-3(5)	2461.2	26.1	7.5	1.0	2.6	2.0	0.3	0.3	33.0	0.7	0.3	0.0	1.6	2.6	0.7	0.0	8.1	11.7	1.6	24.7				
JL-3(7)	2466.1	33.3	3.0	0.3	1.8	1.5	0.8	0.5	0.3	0.8	0.0	1.0	2.8	1.5	3.0	*12.3	7.3	27.0	2.3	41.5				
JL-3(8)	2473.2	37.5	10.8	2.0	5.0	3.3	0.0	0.0	1.0	0.8	0.0	0.5	0.5	1.8	0.8	8.8	4.8	19.0	3.8	35.6				
JL-3(9)	2478.2	41.2	10.0	0.5	2.9	2.2	0.5	0.2	0.0	2.2	0.0	1.0	2.0	1.3	1.0	7.6	2.4	22.0	2.0	36.2				
BK-9 (1)	2303.5	48.3	5.2	5.2	0.8	3.5	0.5	2.2	1.7	10.5	0.0	0.0	1.5	1.2	0.3	0.5	1.5	10.8	3.6	15.7			24.9	504
BK-9 (2)	2304.6	45.8	4.3	5.9	3.5	3.5	0.6	1.9	3.5	8.7	0.0	0.0	0.9	2.4	0.5	0.6	1.4	11.9	4.7	17.7			27.1	614
BK-9 (3)	2305.2	28.0	15.8	8.3	2.7	3.0	4.3	3.0	0.7	2.7	0.0	0.0	1.5	3.7	1.7	0.2	0.0	20.8	3.3	27.9			27.8	1230
BK-9 (4)	2305.8	37.3	10.0	10.8	5.3	1.8	1.0	0.8	0.0	0.5	0.0	0.0	2.3	0.3	0.3	1.0	0.8	23.8	4.3	28.3				
BK-9 (5)	2306.4	38.5	5.7	8.3	1.8	4.6	1.4	2.1	2.9	4.0	0.0	0.0	1.3	1.6	0.2	0.8	2.4	11.9	6.4	18.1				
BK-9 (6)	2307.0	34.0	10.0	7.5	1.0	0.7	0.8	1.3	0.3	2.8	0.0	0.0	1.2	0.5	0.3	37.0	1.8	0.2	0.3	41.0	-9.5	-6.9		
BK-9 (7)	2307.9	26.0	15.2	8.7	2.5	1.5	0.8	1.8	0.2	3.2	0.0	0.0	2.0	2.2	2.3	1.3	0.5	25.5	5.3	33.8				
BK-9 (8)	2308.8	33.2	6.2	5.5	3.5	2.7	2.0	1.5	1.3	3.3	0.0	0.0	3.7	4.3	0.5	0.5	0.0	23.2	5.7	32.1				
BK-9 (9)	2309.2	45.3	1.9	3.6	0.8	1.6	4.3	4.4	2.3	6.1	0.0	0.0	1.7	0.8	0.8	1.8	2.1	13.1	5.1	20.3				
BK-9 (10)	2310.7	43.7	1.9	1.6	1.4	0.5	2.0	3.7	1.4	3.0	0.0	0.0	1.4	0.3	0.0	31.2	6.7	0.5	0.8	40.1				
BK-9 (11)	2312.8	35.0	9.5	10.3	6.8	4.3	2.0	2.5	0.5	4.0	0.5	0.0	1.8	0.8	0.3	0.5	0.8	19.3	1.3	23.3				
BK-9 (12)	2313.5	33.0	11.3	9.3	3.2	1.5	1.3	1.0	3.8	1.2	0.0	0.0	3.2	1.5	0.7	23.8	0.7	0.0	4.5	29.9			7.5	1.4
BK-9 (13)	2314.2	30.3	13.3	9.7	2.3	2.8	3.5	1.7	0.0	2.5	0.0	0.0	4.2	3.2	1.2	0.8	0.2	21.2	1.8	30.8				
BK-9 (14)	2317.2	38.4	4.2	3.6	2.6	1.0	2.6	6.5	0.7	4.7	0.0	0.0	2.6	2.4	0.3	0.2	2.9	16.0	10.7	24.5				
BK-10 (1)	2317.7	36.5	14.8	6.5	4.0	4.3	1.8	1.5	0.0	2.0	0.0	0.0	3.5	1.5	1.0	0.0	1.0	14.8	6.5	21.8				
BK-10 (2)	2918.5	53.5	3.7	2.0	2.0	2.4	3.7	9.7	0.1	1.5	0.0	0.0	0.7	0.2	0.2	0.0	0.0	16.6	5.5	17.7			25.0	310
BK-10 (3)	2921.7	56.0	2.0	0.9	0.9	6.6	1.1	3.1	0.1	1.6	0.0	0.0	0.6	1.2	0.6	0.6	10.9	8.6	4.8	22.6			18.1	44
BK-10 (4)	2922.3	43.7	1.9	1.6	1.6	1.4	2.0	3.7	0.5	3.0	0.0	0.0	1.4	0.3	0.0	31.2	6.7	0.5	0.8	40.1				
BK-10 (5)	2925.8	42.9	7.6	4.9	4.9	4.9	5.4	5.8	1.6	5.4	0.0	0.0	1.5	0.7	0.2	1.0	2.6	8.4	2.8	14.3			26.0	272
BK-10 (6)	3170.8	44.9	3.9	5.5	5.5	6.6	0.9	2.0	0.2	4.2	0.0	0.0	1.8	1.8	0.4	0.7	3.1	14.9	6.4	22.8			20.0	107
BK-10 (7)	3173.0	54.5	0.9	1.9	1.9	5.5	1.4	5.7	0.4	0.9	0.0	0.0	1.4	2.9	0.1	1.4	4.6	12.2	5.5	22.7			21.0	189
BK-10 (8)	3174.2	49.1	3.8	2.2	2.2	3.3	0.5	1.7	0.2	5.2	0.0	0.0	1.7	2.5	0.0	1.8	0.8	16.0	8.7	22.9			20.0	168
BK-10 (9)	3176.0	46.3	4.1	0.9	0.9	5.2	3.4	3.2	0.9	7.7	0.0	0.0	1.8	2.7	0.4	0.4	2.5	14.3	4.8	22.0			25.0	163
BK-10 (10)	3176.3	47.1	2.8	0.8	0.8	6.3	2.4	2.4	0.8	5.7	0.0	0.0	0.8	2.4	0.3	0.2	3.1	16.3	7.0	23.1				
BK-10 (11)	3177.8	48.6	6.8	4.0	4.0	3.6	2.5	2.1	1.5	6.6	0.0	0.0	1.7	1.7	0.3	0.8	0.8	13.6	1.8	18.9			18.0	99

895

Table 2 (part 2)

Well	Depth (m)	Quartz monocrystalline	Quartz polycrystalline	Chert	K-feldspar	Plagioclase	Detrital Biotite	Detrital muscovite	Lithics-sedimentary	Lithics metamorphic	Lithics volcanic	Detrital carbonate clasts	Matrix clay	Quartz cement	Chlorite cement	Calcite cement	Clay cements	Primary porosity	Secondary porosity	IGV	$\delta^{13}C$ ‰ VPDB	$\delta^{18}O$ ‰ VPDB	core analysis porosity %	core analysis permeability mD
TT-11(1)	2691.7	30.4	11.6	9.4	3.5	4.3	3.6	2.0	0.7	3.8	0.0	0.4	2.9	1.6	1.2	0.7	1.9	17.2	4.6	25.5			26.0	608
TT-11(2)	2693.5	32.9	11.0	9.7	4.1	3.6	3.8	2.8	0.6	3.6	0.0	0.4	3.3	1.9	1.2	0.8	2.7	14.5	2.7	24.4				
TT-11(3)	2696.1	33.9	12.6	5.2	3.6	4.0	2.2	2.6	0.7	4.5	0.0	0.0	3.3	2.8	1.3	1.3	1.3	17.2	3.2	27.2				
TT-11(4)	2696.3	30.2	14.3	9.2	3.7	4.3	3.2	1.7	0.5	3.3	0.0	0.3	2.2	3.8	1.2	0.3	0.0	20.0	1.8	27.5				
TT-11(5)	2697.0	30.7	12.6	11.0	3.9	3.8	3.3	2.3	0.6	3.5	0.0	0.4	2.5	4.1	0.7	1.3	1.3	14.7	3.9	24.6				
TT-11(6)	2698.4	30.3	12.7	9.2	3.5	3.8	3.7	2.7	0.5	3.4	0.0	0.3	3.1	4.9	0.7	0.7	2.3	13.9	4.2	25.6				
TT-11(7)	2701.1	32.1	11.2	10.0	4.0	3.5	2.2	1.7	0.8	3.3	0.0	0.8	3.9	5.3	0.9	1.4	2.9	13.0	2.5	27.4			5.0	3
TT-11(8)	2707.5	30.6	15.1	7.3	4.7	3.0	2.2	0.6	1.8	4.8	0.0	0.0	5.5	6.2	0.3	1.5	3.3	12.0	0.9	28.8			24.0	410
TT-11(9)	2708.9	31.7	13.1	8.6	3.4	3.7	2.2	1.3	0.9	3.7	0.0	0.0	2.8	3.9	0.4	5.1	2.8	13.3	2.7	28.3			23.0	350
TT-11(10)	2709.4	30.3	10.0	7.3	3.8	2.5	2.1	1.5	1.0	3.7	0.2	1.7	2.7	2.9	1.2	28.0	1.2	0.0	0.4	36.0	-16.2	-8.3	2.8	0.15
TT-11(11)	2710.7	30.7	14.2	8.3	5.0	3.3	2.0	1.8	1.3	4.8	0.0	0.7	2.5	3.0	1.2	0.3	0.7	17.0	3.0	24.7			23.0	365
TT-11(12)	2711.2	34.7	8.8	8.0	2.8	2.6	2.9	4.1	1.6	3.7	0.0	0.4	2.6	3.9	0.4	0.8	3.1	14.7	4.9	25.5			20.6	9.6
TT-11(13)	2712.7	35.0	12.1	8.0	3.8	3.6	2.6	1.5	1.1	4.5	0.0	0.9	3.4	2.6	0.4	1.1	2.6	14.8	1.7	24.9				
TT-11(14)	2718.6	31.6	4.4	8.7	1.6	0.5	2.1	1.6	0.7	0.7	0.0	2.6	8.7	0.7	0.7	24.0	1.3	5.5	4.1	40.9	-8.2	-11.0		
TT-11(15)	2723.9	34.0	7.2	8.3	2.2	0.6	3.7	0.4	1.0	2.8	0.0	0.9	9.5	1.5	1.3	2.1	1.9	14.9	7.1	31.2			21.0	269
TT-11(16)	2724.8	33.1	7.8	8.0	2.0	0.9	2.3	0.7	0.8	2.5	0.3	0.5	8.3	3.8	0.5	0.0	3.0	15.0	10.0	30.6				
TT-11(17)	2725.4	33.2	7.6	8.1	1.6	1.3	4.9	2.3	0.3	2.3	0.0	0.8	7.1	2.0	1.9	1.8	3.0	15.7	5.8	31.5				
TT-11(18)	2728.7	33.2	6.0	8.0	1.2	1.2	14.0	5.3	0.2	0.5	0.0	0.3	13.0	1.0	1.7	6.5	0.5	6.2	0.5	28.9			12.3	13
TT-11(19)	2729.8	33.9	6.4	7.5	2.9	1.6	5.6	4.0	0.8	2.4	0.0	0.6	8.3	2.1	1.6	1.0	2.4	14.3	4.3	29.7				
TT-11(20)	2735.3	32.5	12.5	8.7	4.4	2.9	1.0	1.4	0.7	3.1	0.5	0.0	3.1	2.4	1.4	3.8	3.1	14.3	4.0	28.1				
TT-11(21)	2742.7	33.8	12.0	7.0	3.3	3.8	3.8	2.0	0.8	3.0	0.0	0.5	3.5	4.3	1.0	1.8	3.8	9.8	6.3	24.2				
TT-11(22)	2747.2	32.8	12.0	8.2	3.3	4.6	3.9	3.0	0.3	2.6	0.0	0.3	3.3	3.3	0.7	0.5	1.3	14.3	5.6	23.4				
TT-11(23)	2748.8	32.3	12.5	7.8	3.7	4.7	3.7	3.0	0.3	2.8	0.2	0.2	2.9	4.7	1.3	0.2	0.0	15.0	4.7	24.1			20.1	176
TT-11(24)	2749.3	36.2	10.2	8.7	2.6	2.4	2.9	2.1	0.9	3.9	0.0	0.0	3.3	2.5	0.9	1.3	2.9	13.8	5.3	24.7				
TT-11(25)	2749.9	34.5	13.5	7.8	3.0	2.6	3.9	3.0	0.9	3.3	0.0	0.0	1.7	2.7	0.5	0.9	1.7	14.7	4.7	22.2				
TT-11(26)	2783.7	36.9	10.5	6.8	1.8	2.6	2.3	4.3	0.5	3.1	0.0	0.5	3.1	3.1	0.8	3.5	3.3	13.0	3.8	26.8			20.0	88
TT-11(27)	2786.5	34.8	14.8	8.4	1.5	1.7	2.2	2.0	0.5	2.5	0.0	0.7	6.2	4.2	1.5	3.5	5.4	7.5	2.5	28.3				
TT-11(28)	2787.1	35.4	11.0	7.5	2.8	1.3	2.9	1.9	0.9	2.8	0.0	0.0	2.3	4.7	0.2	2.6	5.1	14.0	4.9	28.9				
TT-11(29)	2789.9	34.8	15.5	8.8	2.2	1.5	0.5	0.7	0.2	2.7	0.0	0.0	1.2	1.2	0.7	28.0	1.0	0.0	1.0	32.1				
TT-15(1)	2656.0	39.7	6.6	6.2	4.0	2.4	2.1	2.1	0.7	3.9	0.2	0.0	2.7	1.3	1.3	0.2	4.6	16.5	5.3	26.6			20.3	58.5
TT-15(2)	2657.3	34.3	9.2	5.5	4.6	3.5	5.1	4.5	0.8	3.3	0.0	0.3	1.4	2.3	0.8	0.2	4.0	15.8	4.1	24.5			20.5	76.6
TT-15(3)	2658.3	44.7	4.2	3.2	2.8	2.6	1.3	3.1	0.8	3.2	0.0	0.3	3.1	2.3	0.5	1.1	4.5	17.3	4.3	28.8			22.4	59.2
TT-15(4)	2659.0	38.1	6.6	6.7	2.7	2.2	2.2	1.6	1.0	3.1	0.0	1.2	2.5	2.5	1.0	0.8	4.5	17.8	5.1	29.1			21.8	34.0
TT-15(5)	2660.0	33.2	6.9	5.8	3.5	1.4	1.9	4.7	0.8	2.6	0.0	0.5	5.4	4.0	0.7	17.0	11.0	0.0	0.9	38.1				
TT-15(6)	2717.6	35.9	12.8	6.2	3.2	2.7	0.3	0.6	0.4	3.4	0.0	0.0	4.1	3.9	0.4	18.0	4.8	0.0	3.9	31.2				
TT-15(7)	3131.3	39.0	7.9	4.1	2.9	2.8	6.1	7.5	1.2	1.2	0.0	0.0	2.3	5.6	1.2	0.6	3.0	9.3	4.8	22.0				
TT-15 (8)	3132.0	40.3	4.6	3.9	3.0	2.4	2.1	1.3	2.1	2.0	0.0	0.0	3.4	3.4	0.4	1.8	3.4	14.2	11.0	26.6				
TT-15(9)	3133.0	35.8	4.8	4.7	2.0	3.8	5.1	4.4	0.8	2.9	0.0	0.5	3.1	4.0	1.1	3.4	4.4	12.8	5.8	28.8				
TT-15(10)	3135.0	36.1	6.5	6.3	2.7	3.1	2.7	3.1	2.7	2.1	0.0	2.1	3.9	2.9	0.4	6.1	1.6	13.3	4.7	28.2			12.0	53.1
TT-15(11)	3137.0	44.7	2.4	1.9	1.9	2.2	1.5	2.4	1.8	2.2	0.0	0.2	4.4	1.8	0.4	3.2	9.5	14.0	5.0	33.3				
Salda Nadi	1770.0															18.3					-11.9	-11.6		
Salda Nadi	2311.0															21.3					-5.8	-9.3		
Salda Nadi	2312.0															27.3					-4.1	-9.0		